
Adaptive Location Hierarchy Learning for Long-Tailed Mobility Prediction

Yu Wang^{1,*}, Junshu Dai^{1,*}, Yuchen Ying¹, Yuxuan Liang², Tongya Zheng^{3,†}, Mingli Song¹

¹Zhejiang University

²The Hong Kong University of Science and Technology (Guangzhou)

³Hangzhou City University

Abstract

Human mobility prediction is crucial for applications ranging from location-based recommendations to urban planning, which aims to forecast users' next location visits based on historical trajectories. Despite the severe long-tailed distribution of locations, the problem of long-tailed mobility prediction remains largely underexplored. Existing long-tailed learning methods primarily focus on rebalancing the skewed distribution at the data, model, or class level, neglecting to exploit the spatiotemporal semantics of locations. To address this gap, we propose the first plug-and-play framework for long-tailed mobility prediction in an exploitation and exploration manner, named **Adaptive LOcation HierArchY** learning (ALOHA). First, we construct city-tailored location hierarchy based on Large Language Models (LLMs) by exploiting Maslow's theory of human motivation to design Chain-of-Thought (CoT) prompts that captures spatiotemporal semantics. Second, we explore the location hierarchy predictions by Gumbel disturbance and node-wise adaptive weights within the hierarchical tree structure. Experiments on state-of-the-art models across six datasets demonstrate the framework's consistent effectiveness and generalizability, which strikes a well balance between head and tail locations. Weight analysis and ablation studies reveal the optimization differences of each component for head and tail locations. Furthermore, in-depth analyses of hierarchical distance and case study demonstrate the effective semantic guidance from the location hierarchy. Our code is publicly available at <https://anonymous.4open.science/r/ALOHA-W93Z/>.

1 Introduction

Human mobility prediction, which aims to forecast an individual's next location based on historical trajectories and behavioral patterns [18, 42], plays a foundational role in many fields such as urban planning, traffic management and epidemic prevention [4, 34, 46]. However, due to privacy constraints, sparse device sampling, and user authorization biases [46], the visit frequency of locations from the collected real-world mobility data exhibits a severe long-tailed distribution, posing significant challenges for robust prediction models.

Existing mobility prediction researches can be categorized into four paradigms: (1) Recurrent Neural Network (RNN)-based models [9, 30, 42] process check-in sequences through stepwise hidden state propagation, capturing localized dependencies. (2) Graph Neural Network (GNN)-based models [27, 37, 40, 43–45] encode temporal transitions and spatial relationships through graph neural networks. (3) Transformer-based models [10, 31, 40, 43] employ self-attention mechanisms to dynamically weigh pairwise token interactions across entire sequences, enabling global dependencies. (4) Diffusion-based models [21, 26] learn intricate behavior distributions via iterative denoising.

*Equal contribution.

†Corresponding author (doujiang_zheng@163.com).

While these approaches advance sequential modeling, they universally overlook the intrinsic long-tailed distribution of location visits, leading to biased predictions favoring head locations.

Long-tailed learning has been extensively studied in deep learning scenarios, such as Computer Vision (CV) and Recommendation Systems (RecSys). CV methods primarily address class imbalance through data balancing [25, 28], loss function [7, 19], or logit adjustment [23]. RecSys methods extract the shared knowledge across items leveraging meta-learning [38] or transfer learning [47]. While these advanced methods rebalance the skewed distribution of classes at the data, model or class level, they do not inherently account for the spatiotemporal semantics among long-tailed locations. LoTNext [39] represents the first attempt to construct a comprehensive pipeline for long-tailed mobility prediction, incorporating long-tailed graph adjustment and loss adjustment modules. However, its integration of location representation and prediction limits the adaptability of various state-of-the-art mobility prediction models, thereby restricting its broader applicability.

Therefore, we aim to develop a lightweight plug-and-play framework for various mobility prediction models that characterizes the spatiotemporal semantics beyond the long-tailed location distribution. However, achieving this goal presents two major challenges: (1) *How to effectively exploit spatiotemporal semantics from locations without inheriting the long-tailed bias?* We are inspired to utilize objective Large Language Models (LLMs) based on Maslow’s theory of human motivation to capture the high-order location relationships along with the underlying mechanism of human mobility. (2) *How to explore knowledge beyond long-tailed mobility data with lightweight multi-level semantic learning?* This requires us to effectively mitigate distributional bias while simultaneously maintaining model efficiency through a comprehensive approach to multi-level semantic balancing.

To address these challenges, we propose Adaptive **L**ocation **H**ierarchy learning (ALOHA), a long-tailed learning plugin applicable to various models. Specifically, we introduce coarse-grained semantic groupings via a hierarchical tree structure based on Maslow’s theory of human motivation [22] to rebalance the optimization process in an architecture-agnostic manner. First, we construct city-tailored hierarchy by exploiting Maslow’s theory with urban characteristics using LLMs and designed Chain-of-Thought (CoT) prompts. Second, we explore hierarchical location predictions to fully capture the complex spatiotemporal semantics across locations, optimized by Adaptive Hierarchical Loss (AHL) integrating two components: (1) Gumbel disturbance to rebalance the learning of head and tail locations. (2) Adaptive weights for node-wise adjustments to both head and tail nodes at each level. These components effectively foster exploration of mobility knowledge. In conclusion, our main contributions are summarized as follows:

- We propose the first architecture-agnostic plugin for long-tailed mobility prediction, which decouples hierarchical behavior modeling from backbone network design.
- We leverage LLMs and designed CoT prompts based on Maslow’s theory of human motivation to automatically derive city-tailored hierarchical behavioral semantics.
- We introduce an adaptive hierarchical loss that unifies knowledge exploitation with knowledge exploration to mitigate long-tailed location learning challenges.
- Our proposed ALOHA significantly outperforms advanced baselines by up to 9.23%. In-depth analyses further reveal the underlying mechanisms in detail for head and tail locations.

2 Related Work

Mobility Prediction. Existing mobility prediction methods can be categorized into four groups: RNN-based models [9, 30, 42], GNN-based models [27, 37, 40, 43–45], Transformer-based models [10, 31, 40, 43] and Diffusion-based models [21, 26]. Despite their excellent ability to model complex spatiotemporal semantics, they overlook the inherent long-tailed distribution of location visits, resulting in predictions biased toward frequent (head) locations. LoTNext [39] presents the first attempt to explicitly address long-tailed mobility prediction, while it exhibits limited applicability across various backbone architectures. Our proposed plugin framework addresses this limitation leveraging knowledge exploitation and exploration of human mobility.

Long-Tailed Learning. Long-Tailed Learning (LTL) has been extensively studied in deep learning scenarios, such as CV [8, 32] and RecSys [17]. Data balancing [6, 28], logit adjustment [23, 33, 36] and loss function [7, 19, 24] are common LTL techniques in CV field. In RecSys field, the long-tailed problem is more acute [1, 20] as the number of items often vastly exceeds users. Meta-learning [38]

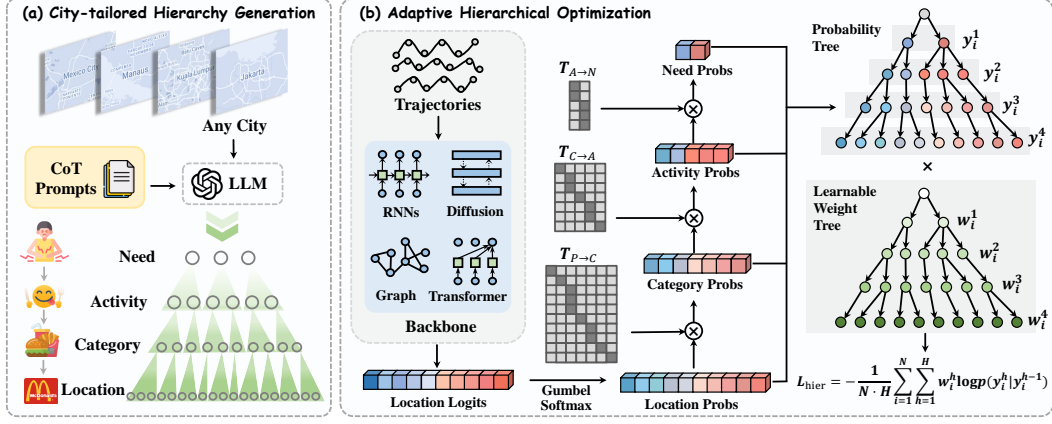


Figure 1: The architecture of ALOHA for long-tailed mobility prediction.

and transfer learning [47] have been employed to address cold-start challenges. However, mobility prediction introduces additional complexity due to dynamic spatiotemporal semantics, limiting the efficacy of these LTL methods on human mobility prediction task.

LLM for Mobility. Currently, several studies [11, 12, 14, 15, 35, 41] utilize LLMs to enhance human mobility learning by designing diverse prompts for LLM-based mobility prediction or integrating LLMs into agent frameworks and spatiotemporal models for mobility generation. LLM-Mob [35] explores prompt engineering by using historical stays and context-aware information for interpretability of mobility prediction. LLMob [14] utilizes CoT reasoning capabilities of LLMs to achieve mobility generation. However, these approaches do not primarily focus on long-tailed mobility predictions.

3 Problem Definition

Let $\mathcal{U} = \{u_i, i \in |\mathcal{U}|\}$ denote the user set and $\mathcal{P} = \{l_i, i \in |\mathcal{P}|\}$ represent the location set, where $l_i = \langle lat, lon \rangle$ specifies geographic coordinates. Here $|\mathcal{U}|$ and $|\mathcal{P}|$ is the number of users and locations, respectively. Each check-in record is defined as $\langle u, l, cat, t \rangle$, where cat is the category of l , indicating that user u visits location l at time t . We formalize the following definitions.

Definition 1 (Trajectory) A trajectory $\mathbf{x} = \{\mathbf{x}_t, t \in |T|\}$ comprises a sequence of spatiotemporal points, where $|T|$ denotes the length of trajectory. Each point $\mathbf{x}_t = \langle l, cat, t \rangle$ represents a visit by user u . The complete trajectory set is $\mathcal{X} = \{\mathbf{x}^m, m \in [M]\}$, containing $|M|$ trajectories.

Definition 2 (Head and Tail Locations) Sorting locations by visit frequency in descending order, we partition them via the Pareto principle [2]: the top 20% frequent locations constitute the head group \mathcal{P}_{head} , while the remaining 80% form the tail group $\mathcal{P}_{tail} = \mathcal{P} \setminus \mathcal{P}_{head}$.

Definition 3 (Mobility Prediction) Given the historical trajectory $\mathbf{x}_{1:t}$ of user u , we aim to predict probability distribution over all locations $|\mathcal{P}|$ to generate a ranked list of locations \mathbf{y}_{t+1} for the next visit. The objective emphasizes improving prediction performance for \mathcal{P}_{tail} .

4 Methodology

In this paper, we design a plug-and-play framework for broader applicability of advanced mobility prediction approaches, named ALOHA. As shown in Figure 1, it comprises two core modules: (a) City-tailored Hierarchy Generation which creates hierarchical labels for arbitrary cities using an LLM with designed CoT prompts and (b) Adaptive Hierarchical Optimization that improves model-agnostic mobility representations through the Adaptive Hierarchical Loss (AHL). We provide a theoretical analysis comparing the gradient optimization of AHL with conventional cross-entropy loss.

4.1 City-tailored Hierarchy Generation

The long-tailed distribution of location visits causes models to prioritize frequent locations during optimization, exacerbating prediction inequity. To mitigate distributional biases, we introduce coarse-

grained semantic groupings via a hierarchical tree structure grounded in Maslow’s theory of human motivation [22], rebalancing the optimization process. Behavioral psychology posits that human mobility inherently reflects need-driven decision-making: personal needs motivate activities, which occur at specific location categories, ultimately manifesting as visits to specific locations. Although human mobility may be influenced by factors like weather and events, this study primarily focuses on the need factor, as it encompasses most motivations for mobility. Consequently, our hierarchy spans four granularity levels: Need \rightarrow Activity \rightarrow Category \rightarrow Location.

Definition of Hierarchical Labels. Our hierarchical structure assigns each location prediction \mathbf{y}_{t+1} to multi-granularity labels $\{y_{t+1}^h \mid h \in [1, H]\}$, where $H = 4$. Each label $y_{t+1}^h \in \{1, 2, \dots, C^h\}$ corresponds to the h -th level, where C^h denotes the class number at this level. Label granularity increases with h (i.e., $C^{h-1} < C^h$), where $C^H = \mathcal{P}$. As outlined in Definition 1, the original trajectories \mathcal{X} inherently contain location-level labels $y^H = \{l_i \mid i \in [1, C^H]\}$ and category-level labels $y^{H-1} = \{cat_i \mid i \in [1, C^{H-1}]\}$. Thus, our focus turns to deriving coarser-grained labels: (1) **activity-level labels** are derived from Foursquare,¹ comprising ten classes. (2) **need-level labels** are adapted from Maslow’s theory, focusing on three fundamental human motivations: physiological needs (survival necessities such as food and shelter), safety needs (security-driven needs including education and employment), and social needs (such as recreational or social activities). Higher-order needs (esteem, self-actualization) are excluded due to their abstract, long-term nature, which lacks empirical observability in mobility data. The proposed hierarchical tree structure implements Maslow’s theory in a more flexible manner, departing from the original rigid order.

Relations of Adjacent-level Labels. We construct transition matrices between adjacent-level labels from bottom to top. Each transition matrix $T_{h \rightarrow h-1}$ quantifies the likelihood of finer-grained labels at level h being mapped to coarser-grained labels at level $h - 1$. The location-to-category transition matrix $T_{H \rightarrow H-1}$ is directly extracted from raw trajectory sequences \mathcal{X} . For the category-to-activity transition matrix $T_{H-1 \rightarrow H-2}$, we leverage LLMs (GPT-4o mini) with designed CoT prompts (Appendix B) to infer mappings between category-level labels (241~330 classes for different cities) and activity-level labels (10 classes applicable to all cities). This LLM-grounded approach not only enhances the mapping accuracy but also addresses the challenges posed by the variability in category definitions across different urban contexts. Three domain experts (two doctoral candidates and a postdoctoral researcher with backgrounds in psychology and behavioral sciences) validate the mappings generated by LLMs in accordance with established annotation protocols [29]. Further details can be found in Appendix B. This hybrid approach minimizes manual effort while ensuring reliability. The activity-to-need transition matrix $T_{H-2 \rightarrow H-3}$ follows the same derivation procedure. Finally, we obtain a four-tier hierarchy for each city shown in Fig 1(a).

4.2 Adaptive Hierarchical Optimization

In this section, we elucidate the adaptive hierarchical optimization module, which integrates knowledge exploitation and exploration of human mobility. To fully exploit the inherent knowledge of mobility patterns, predictions are extended from the single location level to four hierarchical levels, leveraging shared semantics across locations. Then knowledge exploration is performed through two components: (1) Gumbel disturbance rebalances the learning of tail and head classes, enhancing predictions for underrepresented tail locations while maintaining performance of head locations. (2) Adaptive weights promote node-wise adaptation within the hierarchical tree structure, ensuring responsiveness to both tail and head classes at each level. This module enables a nuanced learning of the complex spatiotemporal dynamics of human mobility.

Specifically, we extend the original mobility prediction task in Definition 3 to learn the unknown hierarchical classification distribution based on the hierarchical labels of human motivation:

$$p(\mathbf{y}_{t+1} \mid \mathbf{x}_{1:t}) = p(y_{t+1}^1, \dots, y_{t+1}^H \mid \mathbf{x}_{1:t}). \quad (1)$$

Our framework first derives the finest-grained prediction $p(y_{t+1}^H \mid \mathbf{x}_{1:t})$ using state-of-the-art mobility prediction methods with diverse backbone architectures, including RNN, GNN, Transformer and Diffusion models. Subsequently, the coarse-grained predictions from y_{t+1}^{h-1} to y_{t+1}^h are recursively generated via hierarchical transition matrices in a bottom-up manner, as illustrated in Fig 1(b). This hierarchical classification pipeline offers three core advantages:

¹<https://docs.foursquare.com>

- **Consistency:** Directly computing coarse-grained classifications using hierarchical transition matrices eliminates noise propagation from conflicting supervisory signals.
- **Effectiveness:** Our framework prioritizes fine-grained classification as the primary task, while coarser-grained predictions serve as auxiliary constraints to mitigate granularity competition[3].
- **Efficiency:** Predictions at the coarse-grained level are derived directly through transition matrices, eliminating reliance on the parameters of the coarse-grained classifiers.

Gumbel Disturbance. To mitigate the skewed optimization towards head locations in deep learning models for long-tailed mobility data, we introduce Gumbel disturbance to enhance the exploration of human mobility knowledge. By injecting randomness into the sampling process, Gumbel disturbance enables the model to consider various locations rather than relying solely on high-probability predictions. Notably, the Gumbel distribution is a family of highly stable distributions [13], which preserves the original probability distribution even after noise is added.

Specifically, the fine-grained representation from any backbone architecture is mapped to logits:

$$\mathbf{z} = \text{Backbone}(\mathbf{x}_{1:t}) = \{z_1, z_2, \dots, z_{|\mathcal{P}|}\}, \quad (2)$$

where $\text{Backbone}(\cdot)$ refers to a mobility prediction approach. Subsequently, these logits generate probabilities of leaf nodes in the hierarchical tree using Gumbel-Softmax function:

$$p_0(y_{t+1}^H | \mathbf{x}_{1:t}) = \text{GumbelSoftmax}(z_i) = \frac{\exp((z_i + g_i)/\tau)}{\sum_{j=1}^{C^H} \exp((z_j + g_j)/\tau)}, \quad (3)$$

where i denotes the index of label y_{t+1}^H , τ is a temperature parameter and $g_i = -\log(-\log(a_i))$ is the noise sampled from $a_i \sim \text{Uniform}(0, 1)$. Level-wise prediction $p_0(y_{t+1}^{h-1})$ is then recursively derived in a bottom-up manner (*i.e.*, from fine to coarse granularity) using transition matrices:

$$p_0(y_{t+1}^{h-1}) = T_{h \rightarrow h-1} p_0(y_{t+1}^h), \quad (4)$$

where $T_{h \rightarrow h-1}$ is a transition matrix with a size of $C^h \times C^{h-1}$, the elements of $T_{h \rightarrow h-1}$ are in $\{0, 1\}$ and each row sums to one. In our hierarchical tree structure, the probability of leaf node y_{t+1}^H corresponds to a unique factorization along the path connecting the root node to y_{t+1}^H in a top-down manner, as illustrated in Fig 1(b). Mathematically, y_{t+1}^H is factorized using the chain rule [5] as:

$$p(y_{t+1}^H) = \prod_{h=1}^H p(y_{t+1}^h | y_{t+1}^{h-1}), \quad (5)$$

where H is the depth of the node and $p(y_{t+1}^h | y_{t+1}^{h-1})$ represents the conditional probability of a child node given its parent. The probability of the root node $p(y_{t+1}^0)$ is omitted, as it equals 1. The conditional probability is expressed in terms of the leaf node class probabilities as follows:

$$p(y_{t+1}^h | y_{t+1}^{h-1}) = \frac{\sum_{y_j^H \in \text{Leaves}(y_{t+1}^h)} p_0(y_j^H)}{\sum_{y_j^H \in \text{Leaves}(y_{t+1}^{h-1})} p_0(y_j^H)}, \quad (6)$$

where j indexes the H -th level labels C^H and $p(y_{t+1}^h | y_{t+1}^{h-1}) \in [0, 1]$.

Adaptive Weights. Due to the inherently long-tailed distribution of nodes at the location level, the distribution of high-level nodes is also non-uniform. To better explore dynamic mobility knowledge, we adopt node-wise adaptive weights. To prevent granularity competition [3], we assign lower weights to the coarse-grained levels. For simplicity, the weights are initialized with $\{1, 0.75, 0.5, 0.25\}$ from fine to coarse. We employ the Softplus activation function to ensure the positivity of the weights. Therefore, the Adaptive Hierarchical Loss (AHL) is defined as:

$$\begin{aligned} L_{\text{hier}} &= -\frac{1}{M \cdot (T-1) \cdot H} \sum_{m=1}^M \sum_{t=1}^{T-1} \sum_{h=1}^H w_{t+1}^h \log p(y_{t+1}^h | y_{t+1}^{h-1}) \\ &= -\frac{1}{N \cdot H} \sum_{i=1}^N \sum_{h=1}^H w_i^h \log p(y_i^h | y_i^{h-1}) \end{aligned}, \quad (7)$$

where w_i^h is a learnable weight and N is the number of predictions. Optimizing model parameters with AHL enhances per-level classification accuracy and penalizes errors in a hierarchy-aware way.

4.3 Gradient Comparison of AHL and Cross-Entropy Loss

For simplicity, we consider optimizing a single label y_{t+1}^h rather than all samples from trajectory sequences \mathcal{X} . The optimization objectives for standard cross-entropy loss and AHL are defined as:

$$\ell_{ce} = -\log p(y_i^H). \quad (8)$$

$$\ell_{hier} = -\sum_{h=1}^H w_i^h \log p(y_i^h | y_i^{h-1}). \quad (9)$$

For notational clarity, we introduce S_i^h to aggregate the probabilities of the leaf nodes under y_i^h :

$$p(y_i^h | y_i^{h-1}) = \frac{S_i^h}{S_i^{h-1}}, \quad S_i^h = \sum_{y_k^H \in \text{Leaves}(y_i^h)} p_0(y_k^H), \quad (10)$$

The gradients of these two losses with respect to logits z_j are derived as:

$$\frac{\partial \ell_{ce}}{\partial z_j} = p_0(y_i^H) - 1. \quad (11)$$

$$\frac{\partial \ell_{hier}}{\partial z_j} = p_0(y_i^H) \left[\sum_{h=1}^{H-1} \frac{w_i^{h+1} - w_i^h}{S_i^h} + w_i^1 \right] - w_i^H = p_0(y_i^H) \cdot A - w_i^H, \quad (12)$$

where the superscript of H refers to the location level and 1 represents the need level. It can be observed that AHL encapsulates the intra-hierarchy learning of locations $(w_i^{h+1} - w_i^h)/S_i^h$ in a competitive way, indicating that the equal weights across different levels lead to a degradation optimization of $p_0(y_i^H)w_i^1 - w_i^H$. Besides, w_i^1 and w_i^H serve to stabilize coefficients, preventing gradient diminishing during optimization. The progressively decrease of weight initialization across different levels corresponds to a tendency towards shared semantic learning among long-tailed locations.

5 Experiments

5.1 Experimental Settings

Datasets. We conduct extensive experiments on six real-world mobility datasets, sourced from Foursquare,³ where locations with fewer than 15 visits and users with fewer than 100 check-ins are excluded to isolate long-tailed effects and ensure dataset quality [39]. Each user’s check-in sequence is segmented into trajectories using 24-hour intervals. We sort check-ins chronologically for each user and partition the dataset into training, validation, and test sets in an 8:1:1 ratio [43]. Users or locations absent from the training set but present in validation/test sets are excluded during evaluation. The statistics of processed datasets are summarized in Table 1, while the distribution of locations across hierarchy levels is shown in Figure 2. Further details are available in Appendix C.1.

Table 1: Basic dataset statistics.

City	#User	#Loc.	#Record	#Traj.	#Cat.
JKT	2,827	7,240	240,914	40,733	308
KLP	1,528	3,836	139,391	24,015	259
MAO	1,036	3,180	123,861	18,735	241
MOW	3,234	8,963	316,576	50,702	330
SPB	992	3,077	99,832	15,263	253
MEX	2,715	6,862	189,671	36,016	312

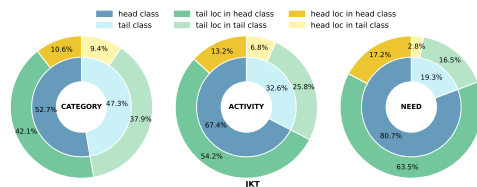


Figure 2: Statistics of locations in hierarchy.

Baselines. We implement four types of backbone architectures for human mobility prediction to validate our framework’s generalizability: RNN-based model (Graph-Flashback [27]), GNN-based model (STHGCN [40]), Transformer-based model (MCLP [31]) and Diffusion-based model (Diff-POI [26]). We compare ALOHA’s performance against two categories of state-of-the-art baselines: (1) widely adopted Long-tailed Learning (LTL) **plugins** in computer vision, including loss function (Focal Loss [19], ClassBalanced Loss [7] and IB loss [24]) and logit adjustment (Post-hoc adjustment [23])

³<https://sites.google.com/site/yangdingqi/home/foursquare-dataset>

and BLV [36]). (2) significant **comprehensive frameworks** for long-tailed recommendation systems (MELT [16]) and human mobility (LoTNext [39]). More details see Appendix C.2.

Evaluation Metrics. We evaluate model performance using $MRR@k$ and $NDCG@k$ with $k \in \{1, 5, 10, 20\}$. $MRR@k$ measures the reciprocal rank of the ground-truth label within the top- k predictions. $NDCG@k$ incorporates positional discounting to prioritize higher-ranked predictions. This metric prioritizes the accurate placement of relevant labels at top ranking positions. The detailed computations of $MRR@k$ and $NDCG@k$ metrics are presented in Appendix C.3.

Table 2: $MRR@k$ performance on the JKT and KLP datasets, with the best results highlighted in red and the second-best results in light red. **Improv.** denotes the percentage of improvement.

Dataset	JKT				KLP			
	MRR@1	MRR@5	MRR@10	MRR@20	MRR@1	MRR@5	MRR@10	MRR@20
Graph-Flashback	0.1916	0.2791	0.2909	0.2962	0.1729	0.2591	0.2703	0.2763
+ Focal	0.1955	0.2800	0.2919	0.2975	0.1853	0.2630	0.2753	0.2817
+ CB	0.1645	0.2387	0.2489	0.2536	0.1502	0.2147	0.2260	0.2309
+ IB	0.1487	0.2205	0.2288	0.2324	0.1318	0.1936	0.2034	0.2070
+ LA	0.1721	0.2474	0.2580	0.2628	0.1522	0.2219	0.2321	0.2372
+ BLV	0.1874	0.2781	0.2897	0.2947	0.1881	0.2680	0.2796	0.2854
+ Ours	0.2042	0.2893	0.3012	0.3066	0.1945	0.2744	0.2854	0.2914
Improv.	4.45%	3.32%	3.19%	3.06%	3.40%	2.39%	2.07%	2.10%
STHGCN	0.1976	0.2768	0.2878	0.2934	0.1961	0.2708	0.2826	0.2880
+ Focal	0.1950	0.2782	0.2878	0.2937	0.1829	0.2602	0.2719	0.2772
+ CB	0.1734	0.2422	0.2519	0.2566	0.1346	0.2006	0.2101	0.2146
+ IB	0.1558	0.2239	0.2316	0.2362	0.0639	0.1056	0.1127	0.1170
+ LA	0.1708	0.2424	0.2518	0.2569	0.1198	0.1942	0.2067	0.2125
+ BLV	0.1966	0.2773	0.2883	0.2935	0.1937	0.2744	0.2858	0.2905
+ Ours	0.2097	0.2899	0.3002	0.3058	0.2065	0.2836	0.2946	0.2996
Improv.	6.12%	4.21%	4.13%	4.12%	5.30%	3.35%	3.08%	3.13%
MCLP	0.1968	0.2796	0.2908	0.2958	0.1833	0.2594	0.2703	0.2755
+ Focal	0.1961	0.2771	0.2881	0.2937	0.1713	0.2508	0.2616	0.2669
+ CB	0.1792	0.2517	0.2621	0.2667	0.1554	0.2237	0.2336	0.2382
+ IB	0.1839	0.2559	0.2649	0.2689	0.1534	0.2171	0.2247	0.2277
+ LA	0.1834	0.2577	0.2679	0.2725	0.1554	0.2258	0.2362	0.2414
+ BLV	0.1918	0.2763	0.2868	0.2927	0.1885	0.2627	0.2725	0.2780
+ Ours	0.2045	0.2860	0.2966	0.3020	0.1937	0.2665	0.2774	0.2827
Improv.	3.91%	2.29%	1.99%	2.10%	2.76%	1.45%	1.80%	1.69%
Diff-POI	0.1234	0.1826	0.1912	0.1949	0.1250	0.1762	0.1843	0.1882
+ Focal	0.1287	0.1865	0.1955	0.1994	0.1242	0.1794	0.1875	0.1921
+ CB	0.1282	0.1826	0.1876	0.1898	0.1078	0.1605	0.1650	0.1674
+ IB	0.0824	0.0981	0.1007	0.1021	0.1166	0.1378	0.1401	0.1419
+ LA	0.1147	0.1677	0.1748	0.1780	0.0998	0.1511	0.1559	0.1595
+ BLV	0.1289	0.1843	0.1928	0.1966	0.1194	0.1707	0.1785	0.1836
+ Ours	0.1408	0.1950	0.2035	0.2067	0.1346	0.1901	0.1970	0.2008
Improv.	9.23%	4.56%	4.09%	3.66%	7.68%	5.96%	5.07%	4.53%
MELT	0.1388	0.2276	0.2399	0.2460	0.1139	0.1962	0.2072	0.2127
LoTNext	0.1779	0.2568	0.2676	0.2724	0.1721	0.2423	0.2534	0.2593

5.2 Main Results

We compare ALOHA with LTL plugin and framework baselines using $MRR@k$ and $NDCG@k$ metrics across six datasets for mobility prediction. Partial results are presented in Table 2, and the complete results are provided in Appendix E.1. We can yield three key observations:

- **Effectiveness and Generalizability of ALOHA.** ALOHA consistently achieves the highest $MRR@k$ on all backbone architectures. Specifically, it attains a 6.12% improvement on GNN-based backbone (STHGCN) and a 9.23% gain on Diffusion-based backbone (Diff-POI) over $MRR@1$ metric of KLP dataset. This superiority arises from ALOHA’s adaptive hierarchical optimization, which mitigates skewed location distributions through shared semantic among locations.
- **Performance of Plugin Baselines.** Although some LTL plugin baselines achieve suboptimal performance on partial metrics (*e.g.*, MCLP + BLV on KLP dataset), their performance is unstable and may even damage the performance of the basic backbones (*e.g.*, a decline of 33.23% on $MRR@1$ for JKT dataset with Diff-POI + IB). This suggests that LTL plugins for computer vision are not competent for mobility prediction involving more complex spatiotemporal modeling.

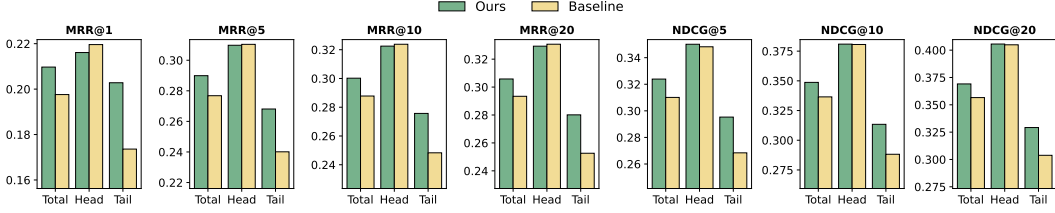


Figure 3: MRR@ k and NDCG@ k comparison between ALOHA and SOTA baseline on JKT dataset.

- Performance of Framework Baselines.** MELT underperforms LoTNext by up to 21.98% on MRR@1 of KLP dataset. This discrepancy arises from the direct transplantation of LTL strategies for ResSys, which fails to address the unique challenges of mobility prediction such as varying scales of distributions, distinct prediction strategies, and the absence of spatial considerations. Although LoTNext outperforms methods based on Diff-POI backbone, it underperforms compared to those utilizing other backbones, highlighting a need for improved generalizability and flexibility.

5.3 Further Analysis

Long-Tail Location Analysis. According to the partitioning process described in Definition 2, locations are categorized into tail and head groups. To assess whether our model enhances performance on long-tailed locations, we compare ALOHA with the optimal baseline method (STHGCN) using the GNN-based backbone architecture on the JKT dataset. Figure 3 demonstrates that ALOHA exhibits significant improvements in total and tail groups. In the head group, performance remains comparable to the baseline at MRR@ k while achieving marginally superior results at NDCG@ k . This outcome indicates that our adaptive hierarchical learning framework effectively enhances the learning process for long-tailed locations without compromising performance on head locations.

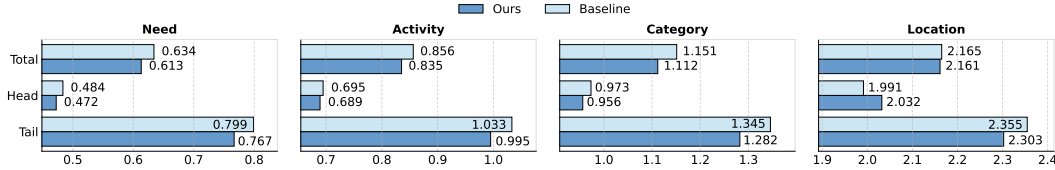


Figure 4: Hierarchical distance comparison between ALOHA and SOTA baseline on JKT dataset.

Hierarchical Distance Analysis. We further evaluate the prediction similarity in relation to the label hierarchy tree, which is computed based on the lowest common ancestor between the ground truth and the predicted location. A smaller hierarchical distance corresponds to less severe prediction errors. We compare ALOHA with the best baseline (*i.e.*, STHGCN) on the JKT dataset. As shown in Figure 4, ALOHA exhibits a smaller hierarchical distance at the coarse-grained levels of need, activity, and category, with total improvements of up to 3.3%, 2.5% and 3.4%, respectively. This indicates that ALOHA better captures shared semantics. This enhancement contributes to its performance regarding the hierarchical distance of long-tailed locations, thereby improving overall performance.

Weights Analysis. We analyze the optimized weights obtained from the “STHGCN + Ours” model on the JKT dataset to gain insights into the adaptive adjustment mechanism for dynamic spatiotemporal semantic modeling. Figure 5 presents the visualization of the optimized weights for head and tail groups across four hierarchical levels. The results indicate that long-tailed classes exhibit a more concentrated weight distribution with significantly larger values compared to head classes, validating the adjustments made for both groups. Additionally, the calculated correlation coefficients reveal markedly higher correlations between adjacent hierarchical levels, demonstrating the effectiveness of the hierarchical structure. In contrast, long-tailed classes show lower correlation coefficients, reflecting their diverse characteristics. These findings highlight the model’s

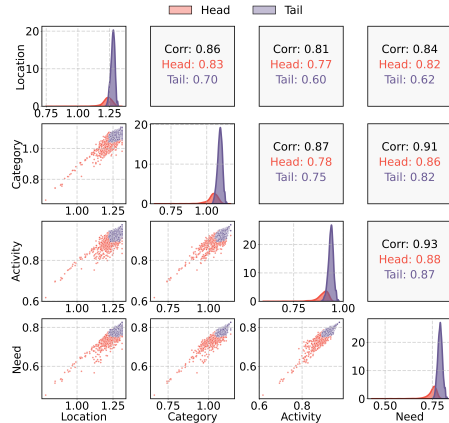


Figure 5: Optimized hierarchical weights.

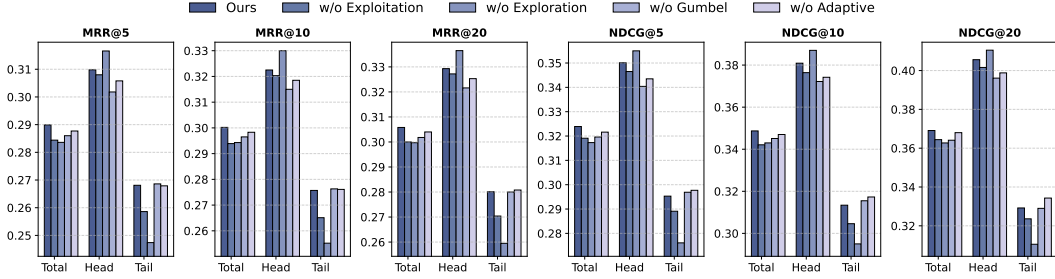


Figure 6: Ablation study of our proposed ALOHA using STHGCN backbone on JKT dataset.

ability to learn effectively from long-tailed locations while leveraging the interrelatedness of head locations, ultimately achieving balanced performance in mobility prediction.

Effect of Different Components. We conduct the following ablation studies: (1) “w/o Exploitation” removes the hierarchical structure and retains only Gumbel disturbance; (2) “w/o Exploration” removes Gumbel disturbance and adaptive weights; (3) “w/o Gumbel” removes only Gumbel disturbance; (4) “w/o Adaptive” removes only adaptive weights. As shown in Figure 6, “Ours” achieves the best performance across total locations and all variants outperform the second-best results presented in Table 2, confirming the effectiveness of ALOHA. “w/o Exploration” performs best on \mathcal{P}_{head} but worst on \mathcal{P}_{tail} , while “w/o Exploitation” underperforms “Ours” in every group, indicating the significance of the hierarchical structure’s exploitation capability and the necessity of rebalancing through the exploration module. “w/o Gumbel” and “w/o Adaptive” result in a slight degradation in performance, demonstrating the superiority of our overall hierarchical framework. Additional results of the ablation studies are available in Appendix E.2.2.

Table 3: Case study on long-tailed location prediction.

Level	Ground Truth	Ours					Baseline				
		No.1	No.2	No.3	No.4	No.5	No.1	No.2	No.3	No.4	No.5
Need	Safety	✓	✓	Physiological	Physiological	✓	Physiological	Social	Physiological	Physiological	Physiological
Act	Community	✓	✓	Dining	Dining	✓	Dining	Entertainment	Dining	Dining	Dining
Cat	Home	✓	College	Mall	Mall	High School	Mall	Multiplex	Mall	Mall	Mall
Loc	6899	✓	67	334	262	48	334	381	262	433	194

Case Study: Prediction on Long-Tail Location. We conduct a case study comparing ALOHA with the SOTA baseline (STHGCN) on the JKT dataset. The true label is a long-tailed location with only twenty-seven visits. The coarse-grained results are derived from transition matrices based on location-level predicted results. As shown in Table 3, ALOHA predicts the true label at rank one, while STHGCN fails to include it among the top five predictions. Notably, ALOHA achieves high accuracy at coarse-grained levels, with the top two predictions aligning in both need and activity levels, thereby enhancing prediction diversity and reliability. In contrast, the baseline prioritizes popular locations (*i.e.*, mall), neglecting less frequented locations. These results demonstrate ALOHA’s effectiveness in identifying long-tailed locations and underscore the baseline’s limitations in producing diverse predictions, emphasizing the significance of the hierarchical structure in location prediction.

6 Conclusion

In this study, we introduce ALOHA, an innovative plugin designed for long-tailed human mobility prediction. Our framework leverages large language models to automatically generate city-tailored location hierarchies based on Maslow’s theory. Furthermore, we present an adaptive hierarchical loss function that effectively exploits mobility knowledge and explores latent probabilities of location visits. Through extensive comparisons with two categories of baselines (*i.e.*, five well-known plugins on four advanced backbones and two comprehensive frameworks), we validate the superiority of ALOHA in terms of effectiveness and generalizability. A potential limitation of our study is that the current framework does not account for additional factors that may influence mobility predictions, such as natural disasters or large-scale events. We aim to investigate this problem in our future work.

References

- [1] Alex Beutel, Ed H Chi, Zhiyuan Cheng, Hubert Pham, and John Anderson. Beyond globally optimal: Focused learning for improved recommendations. In *International World Wide Web Conferences*, pages 203–212, 2017.
- [2] George EP Box and R Daniel Meyer. An analysis for unreplicated fractional factorials. *Technometrics*, 28(1):11–18, 1986.
- [3] Dongliang Chang, Kaiyue Pang, Yixiao Zheng, Zhanyu Ma, Yi-Zhe Song, and Jun Guo. Your "flamingo" is my "bird": Fine-grained, or not. In *IEEE Conference on Computer Vision and Pattern Recognition*, pages 11476–11485, 2021.
- [4] Can Chen, Mengya Yang, Yu Wang, Daixi Jiang, Yuxia Du, Kexin Cao, Xiaobao Zhang, Xiaoyue Wu, Mengsha Chen, Yue You, et al. Intensity and drivers of subtypes interference between seasonal influenza viruses in mainland china: A modeling study. *iScience*, 27(3), 2024.
- [5] Jingzhou Chen, Peng Wang, Jian Liu, and Yuntao Qian. Label relation graphs enhanced hierarchical residual network for hierarchical multi-granularity classification. In *IEEE Conference on Computer Vision and Pattern Recognition*, pages 4858–4867, 2022.
- [6] Ekin D Cubuk, Barret Zoph, Jonathon Shlens, and Quoc V Le. Randaugment: Practical automated data augmentation with a reduced search space. In *Annual Conference on Neural Information Processing Systems*, pages 702–703, 2020.
- [7] Yin Cui, Menglin Jia, Tsung-Yi Lin, Yang Song, and Serge Belongie. Class-balanced loss based on effective number of samples. In *IEEE Conference on Computer Vision and Pattern Recognition*, pages 9268–9277, 2019.
- [8] Yingxiao Du and Jianxin Wu. No one left behind: Improving the worst categories in long-tailed learning. In *IEEE Conference on Computer Vision and Pattern Recognition*, pages 15804–15813, 2023.
- [9] Jie Feng, Yong Li, Chao Zhang, Funing Sun, Fanchao Meng, Ang Guo, and Depeng Jin. Deepmove: Predicting human mobility with attentional recurrent networks. In *International World Wide Web Conferences*, pages 1459–1468, 2018.
- [10] Shanshan Feng, Feiyu Meng, Lisi Chen, Shuo Shang, and Yew Soon Ong. Rotan: A rotation-based temporal attention network for time-specific next poi recommendation. In *ACM Knowledge Discovery and Data Mining*, pages 759–770, 2024.
- [11] Letian Gong, Yan Lin, Yiwen Lu, Xuedi Han, Yichen Liu, Shengnan Guo, Youfang Lin, Huaiyu Wan, et al. Mobility-llm: Learning visiting intentions and travel preference from human mobility data with large language models. *Annual Conference on Neural Information Processing Systems*, 37:36185–36217, 2024.
- [12] Ammar Haydari, Dongjie Chen, Zhengfeng Lai, Michael Zhang, and Chen-Nee Chuah. Mobilitygpt: Enhanced human mobility modeling with a gpt model. *arXiv preprint arXiv:2402.03264*, 2024.
- [13] Eric Jang, Shixiang Gu, and Ben Poole. Categorical reparameterization with gumbel-softmax. *International Conference on Learning Representations*, 2017.
- [14] WANG JIAWEI, Renhe Jiang, Chuang Yang, Zengqing Wu, Ryosuke Shibasaki, Noboru Koshizuka, Chuan Xiao, et al. Large language models as urban residents: An llm agent framework for personal mobility generation. *Annual Conference on Neural Information Processing Systems*, 37:124547–124574, 2024.
- [15] Chenlu Ju, Jiaxin Liu, Shobhit Sinha, Hao Xue, and Flora Salim. Trajllm: A modular llm-enhanced agent-based framework for realistic human trajectory simulation. *arXiv preprint arXiv:2502.18712*, 2025.
- [16] Kibum Kim, Dongmin Hyun, Sukwon Yun, and Chanyoung Park. Melt: Mutual enhancement of long-tailed user and item for sequential recommendation. In *International Conference on Research on Development in Information Retrieval*, pages 68–77, 2023.
- [17] Yejin Kim, Kwangseob Kim, Chanyoung Park, and Hwanjo Yu. Sequential and diverse recommendation with long tail. In *International Joint Conference on Artificial Intelligence*, volume 19, pages 2740–2746, 2019.
- [18] Peibo Li, Maarten de Rijke, Hao Xue, Shuang Ao, Yang Song, and Flora D Salim. Large language models for next point-of-interest recommendation. In *International Conference on Research on Development in Information Retrieval*, pages 1463–1472, 2024.

- [19] Tsung-Yi Lin, Priya Goyal, Ross Girshick, Kaiming He, and Piotr Dollár. Focal loss for dense object detection. In *International Conference on Computer Vision*, pages 2980–2988, 2017.
- [20] Siyi Liu and Yujia Zheng. Long-tail session-based recommendation. In *ACM Conference on Recommender Systems*, pages 509–514, 2020.
- [21] Jing Long, Guanhua Ye, Tong Chen, Yang Wang, Meng Wang, and Hongzhi Yin. Diffusion-based cloud-edge-device collaborative learning for next poi recommendations. In *ACM Knowledge Discovery and Data Mining*, pages 2026–2036, 2024.
- [22] Abraham Harold Maslow. A theory of human motivation. *Psychological review*, 50(4):370, 1943.
- [23] Aditya Krishna Menon, Sadeep Jayasumana, Ankit Singh Rawat, Himanshu Jain, Andreas Veit, and Sanjiv Kumar. Long-tail learning via logit adjustment. In *International Conference on Learning Representations*, 2021.
- [24] Seulki Park, Jongin Lim, Younghan Jeon, and Jin Young Choi. Influence-balanced loss for imbalanced visual classification. In *IEEE Conference on Computer Vision and Pattern Recognition*, pages 735–744, 2021.
- [25] Seulki Park, Youngkyu Hong, Byeongho Heo, Sangdoon Yun, and Jin Young Choi. The majority can help the minority: Context-rich minority oversampling for long-tailed classification. In *IEEE Conference on Computer Vision and Pattern Recognition*, pages 6887–6896, 2022.
- [26] Yifang Qin, Hongjun Wu, Wei Ju, Xiao Luo, and Ming Zhang. A diffusion model for poi recommendation. *ACM Transactions on Information Systems*, 42(2):1–27, 2023.
- [27] Xuan Rao, Lisi Chen, Yong Liu, Shuo Shang, Bin Yao, and Peng Han. Graph-flashback network for next location recommendation. In *ACM Knowledge Discovery and Data Mining*, pages 1463–1471, 2022.
- [28] Jiang-Xin Shi, Tong Wei, Yuke Xiang, and Yu-Feng Li. How re-sampling helps for long-tail learning? *Annual Conference on Neural Information Processing Systems*, 36:75669–75687, 2023.
- [29] Christian Stab and Iryna Gurevych. Annotating argument components and relations in persuasive essays. In *Annual Meeting of the Association for Computational Linguistics*, pages 1501–1510, 2014.
- [30] Ke Sun, Tiejun Qian, Tong Chen, Yile Liang, Quoc Viet Hung Nguyen, and Hongzhi Yin. Where to go next: Modeling long-and short-term user preferences for point-of-interest recommendation. In *AAAI Conference on Artificial Intelligence*, volume 34, pages 214–221, 2020.
- [31] Tianao Sun, Ke Fu, Weiming Huang, Kai Zhao, Yongshun Gong, and Meng Chen. Going where, by whom, and at what time: Next location prediction considering user preference and temporal regularity. In *ACM Knowledge Discovery and Data Mining*, pages 2784–2793, 2024.
- [32] Yingfan Tao, Jingna Sun, Hao Yang, Li Chen, Xu Wang, Wenming Yang, Daniel Du, and Min Zheng. Local and global logit adjustments for long-tailed learning. In *IEEE Conference on Computer Vision and Pattern Recognition*, pages 11783–11792, 2023.
- [33] Junjiao Tian, Yen-Cheng Liu, Nathaniel Glaser, Yen-Chang Hsu, and Zsolt Kira. Posterior re-calibration for imbalanced datasets. *Annual Conference on Neural Information Processing Systems*, 33:8101–8113, 2020.
- [34] Jingyuan Wang, Jiawei Jiang, Wenjun Jiang, Chao Li, and Wayne Xin Zhao. Libcity: An open library for traffic prediction. In *ACM SIGSPATIAL International Conference on Advances in Geographic Information Systems*, 2021.
- [35] Xinglei Wang, Meng Fang, Zichao Zeng, and Tao Cheng. Where would i go next? large language models as human mobility predictors. *arXiv preprint arXiv:2308.15197*, 2023.
- [36] Yuchao Wang, Jingjing Fei, Haochen Wang, Wei Li, Tianpeng Bao, Liwei Wu, Rui Zhao, and Yujun Shen. Balancing logit variation for long-tailed semantic segmentation. In *IEEE Conference on Computer Vision and Pattern Recognition*, pages 19561–19573, 2023.
- [37] Zhaobo Wang, Yanmin Zhu, Chunyang Wang, Wenzhe Ma, Bo Li, and Jiadi Yu. Adaptive graph representation learning for next poi recommendation. In *International Conference on Research on Development in Information Retrieval*, pages 393–402, 2023.
- [38] Chunyu Wei, Jian Liang, Di Liu, Zehui Dai, Mang Li, and Fei Wang. Meta graph learning for long-tail recommendation. In *ACM Knowledge Discovery and Data Mining*, pages 2512–2522, 2023.

- [39] Xiaohang Xu, Renhe Jiang, Chuang Yang, Kaoru Sezaki, et al. Taming the long tail in human mobility prediction. *Annual Conference on Neural Information Processing Systems*, 37:54748–54771, 2024.
- [40] Xiaodong Yan, Tengwei Song, Yifeng Jiao, Jianshan He, Jiaotuan Wang, Ruopeng Li, and Wei Chu. Spatio-temporal hypergraph learning for next poi recommendation. In *International Conference on Research on Development in Information Retrieval*, pages 403–412, 2023.
- [41] Yuwei Yan, Qingbin Zeng, Zhiheng Zheng, Jingzhe Yuan, Jie Feng, Jun Zhang, Fengli Xu, and Yong Li. Opencity: A scalable platform to simulate urban activities with massive llm agents. *arXiv preprint arXiv:2410.21286*, 2024.
- [42] Dingqi Yang, Benjamin Fankhauser, Paolo Rosso, and Philippe Cudre-Mauroux. Location prediction over sparse user mobility traces using rnns. In *International Joint Conference on Artificial Intelligence*, pages 2184–2190, 2020.
- [43] Song Yang, Jiamou Liu, and Kaiqi Zhao. Getnext: trajectory flow map enhanced transformer for next poi recommendation. In *International Conference on Research on Development in Information Retrieval*, pages 1144–1153, 2022.
- [44] Fuqiang Yu, Lizhen Cui, Wei Guo, Xudong Lu, Qingzhong Li, and Hua Lu. A category-aware deep model for successive poi recommendation on sparse check-in data. In *International World Wide Web Conferences*, pages 1264–1274, 2020.
- [45] Jixiao Zhang, Yongkang Li, Ruotong Zou, Jingyuan Zhang, Renhe Jiang, Zipei Fan, and Xuan Song. Hyper-relational knowledge graph neural network for next poi recommendation. *International World Wide Web Conferences*, 2024.
- [46] Liang Zhang, Cheng Long, and Gao Cong. Region embedding with intra and inter-view contrastive learning. *IEEE Transactions on Knowledge and Data Engineering*, 35(9):9031–9036, 2023.
- [47] Yin Zhang, Derek Zhiyuan Cheng, Tiansheng Yao, Xinyang Yi, Lichan Hong, and Ed H Chi. A model of two tales: Dual transfer learning framework for improved long-tail item recommendation. In *International World Wide Web Conferences*, pages 2220–2231, 2021.

A Notations

The notations used in our paper are summarized as follows.

Table 4: Notation Table.

Symbol	Meaning
\mathcal{U}, u	User set and user
\mathcal{P}, l	Location set and location
$\mathcal{P}_{\text{head}}, \mathcal{P}_{\text{tail}}$	Head group and tail group of locations
cat	Category of location
t	Time and position index
$\mathcal{X}, \mathbf{x}, \mathbf{x}_t$	Trajectory set, trajectory, and spatiotemporal point
\mathbf{y}, y	Predicted location set and location
\mathbf{z}, z	Logits and logit
$p_0(\cdot)$	Initial probability of leaf node
$p(\cdot)$	Hierarchical conditional probability
S_i^h	Sum of probabilities of leaf nodes for label y_i^h
w	Learnable weight score
M	Number of trajectories
T	Sequence length
H	Height of hierarchy
C_h	Number of labels at the h -th hierarchical level
$T_{h \rightarrow h-1}$	Transition matrix from the h -th level to the $(h - 1)$ -th level
τ	Temperature parameter
g_i	Sampled noise
r_u	Rank of correctly predicted label for user u
L, ℓ	Total loss for all predictions and loss for a prediction

B Supplement to Method

The prompts used to generate $T(\text{Category} \rightarrow \text{Activity})$ and $T(\text{Activity} \rightarrow \text{Need})$ are as follows.

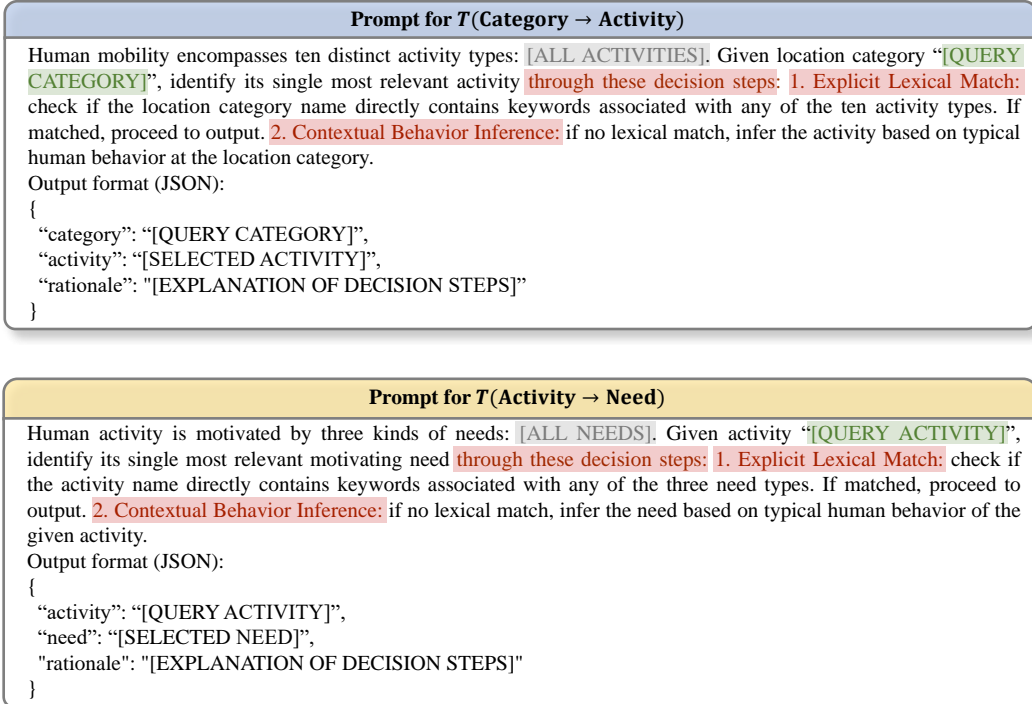


Figure 7: Chain-of-thought prompts for relations of adjacent-level labels.

Evaluation of LLM-generated Mappings. The relations between adjacent-level labels are established by leveraging Large Language Models (LLMs) and our designed Chain-of-Thought (CoT) prompts. To minimize additional noise, we engage three annotators to verify the generated results. All three annotators possess relevant expertise, consisting of two senior Ph.D. candidates and one postdoctoral researcher with backgrounds in psychology and behavioral sciences. We select these experts following studies of annotation tasks in Natural Language Processing (NLP) [29]. Specifically, if three experts disagree on a label, we invite another expert and start a discussion. Through this process, we define the relations from the category level to the activity level, while the relations from the category level to the need level follow the same procedure. This annotation approach aligns with the requirements of our problem settings due to the limited scale of activity types. The integration of LLMs and human expertise minimizes manual effort while ensuring reliability.

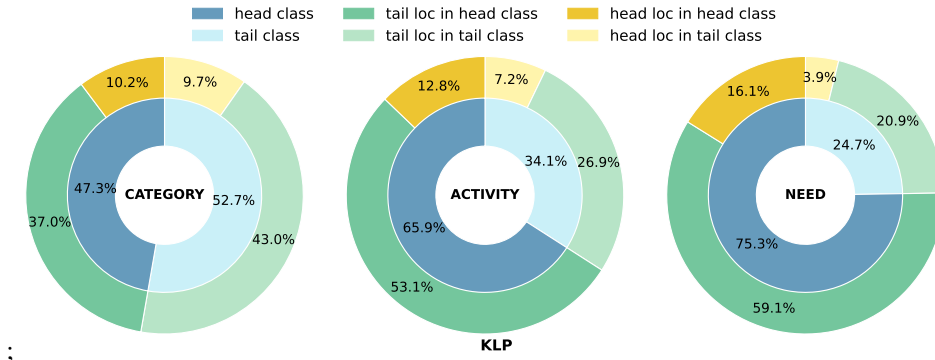


Figure 8: Statistics of locations in the hierarchy on the KLP dataset.

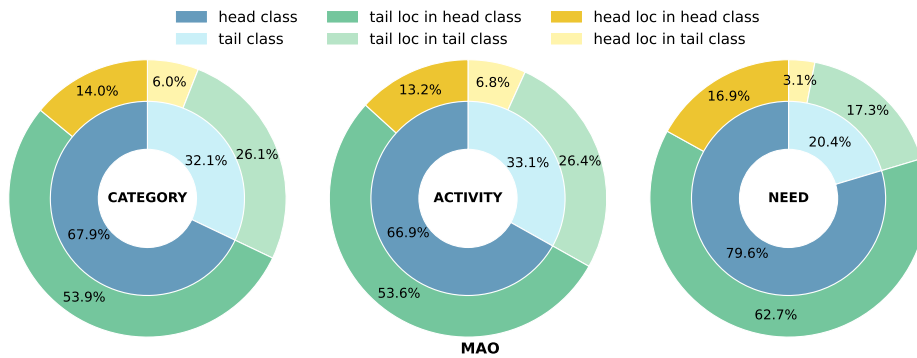


Figure 9: Statistics of locations in the hierarchy on the MAO dataset.

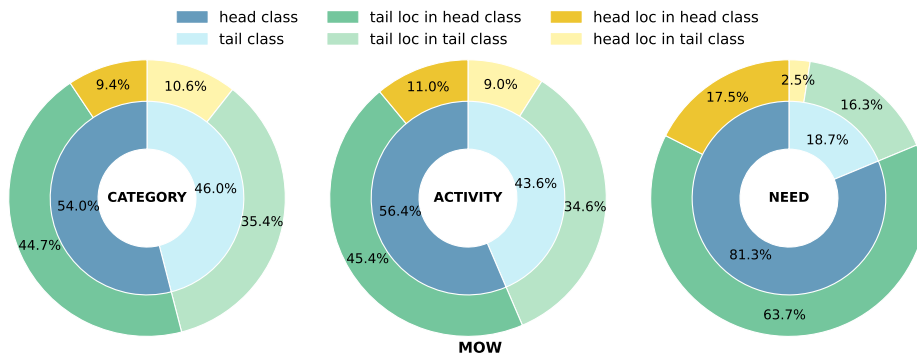


Figure 10: Statistics of locations in the hierarchy on the MOW dataset.

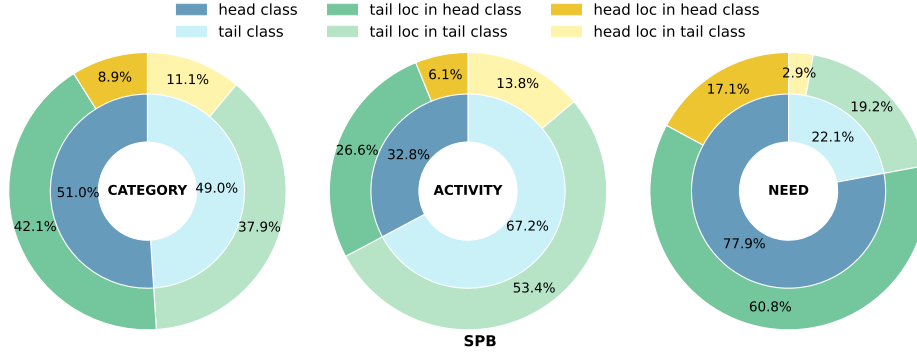


Figure 11: Statistics of locations in the hierarchy on the SPB dataset.

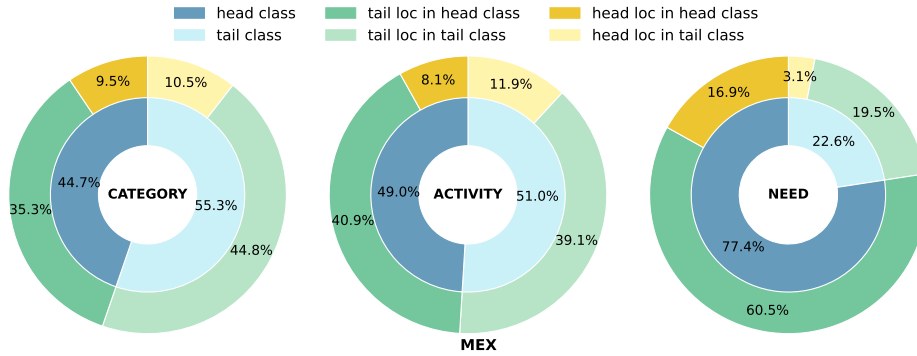


Figure 12: Statistics of locations in the hierarchy on the MEX dataset.

C Experimental Settings

C.1 Datasets

Statistics of Locations in Hierarchy. To visualize the frequency distribution of locations within different hierarchical levels, we calculate the visit frequency of each class across three coarse-grained levels: category, activity, and need. At each hierarchical level, we rank all classes in descending order based on their frequency, designating the top 20% as head classes and the bottom 80% as tail classes. This classification allows us to analyze the representation of head and tail locations at the location level, where the proportions of head and tail locations correspond to those in the head and tail classes identified in the coarse-grained levels. As depicted in Figure 2, 8, 9, 10, 11, and 12, we observe that as the granularity of classification decreases from left to right, the proportions of both head and tail locations within the head class tend to rise significantly, with a particularly pronounced increase in the proportion of tail locations. For instance, in the JKT dataset, the tail class in the activity Level comprises a substantial portion, indicating a diverse range of less-frequented locations. Similarly, this trend is echoed across the other datasets, particularly in KLP and MAO, where a notable percentage of tail locations exists even within the head class. This suggests that while certain locations are more popular, there remains considerable diversity among less-visited locations within a city. This analysis highlights the importance of understanding both the head and tail classes in optimizing location-based services and recommendations.

Distribution of Users and Locations. We present the frequency distribution of users and locations across six human mobility datasets, as illustrated in Figure 13. The results reveal a clear power-law distribution in both user and location frequencies, indicating a long-tailed effect in which a small number of users and locations account for a significant portion of interactions. The curves for users (in red) and locations (in green) are notably similar, particularly in the cities of KLP and MOW, suggesting more uniform exploration behavior among users in these areas. Conversely, cities such as MAO and SPB exhibit a pronounced decline in interaction frequency, implying a concentration of

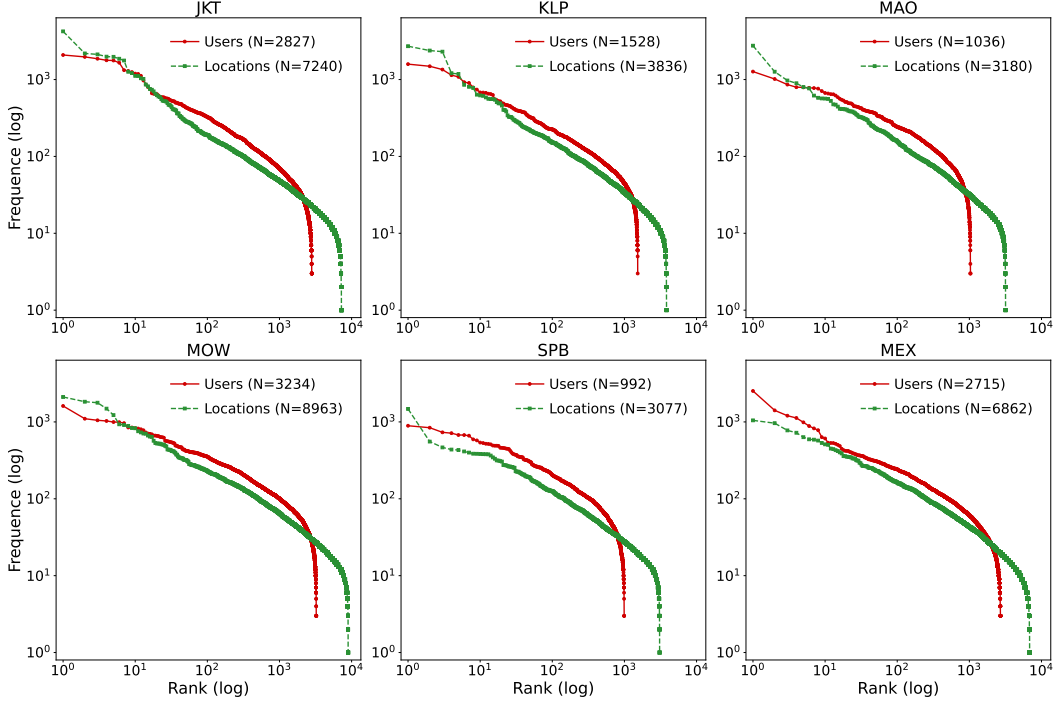


Figure 13: Distribution of users and locations on six datasets.

user visits to a limited number of popular locations. This trend suggests that while some locations attract substantial attention, many others remain under-visited.

C.2 Baselines

We select four advanced mobility prediction approaches involving four types of architectures:

- **Graph-Flashback** [27] utilizes RNNs to capture sequential patterns through embeddings derived from user-POI knowledge graph and location transition graph.
- **STHGCN** [40] combines hypergraph Transformers with spatiotemporal encoding to model intra-user and inter-user trajectories dependencies.
- **MCLP** [31] integrates topic modeling for location preferences, an arrival time estimator for time embeddings, and Transformer architecture for mining sequential patterns.
- **Diff-POI** [26] employs dual graph encoders for spatiotemporal features, augmented by Diffusion-based sampling for spatial trend prediction.

We compare ALOHA’s performance against two categories of state-of-the-art baselines: (1) five widely adopted long-tailed learning **plugins**:

- **Focal Loss** (Focal) [19] aims to address the extreme imbalance between foreground and background classes by reshaping the standard cross-entropy loss. This reshaping down-weights the loss assigned to well-classified examples, thereby focusing training on a sparse set of challenging instances and preventing the vast number of easy negatives from overwhelming the detector during training.
- **ClassBalanced Loss** (CB) [7] introduces a novel theoretical framework for measuring data overlap by associating each sample with a small neighboring region rather than a single point. It implements a re-weighting scheme that employs the effective number of samples for each class to rebalance the loss, thereby yielding a class-balanced loss.
- **IB Loss** (IB) [24] proposes a balanced training method to address challenges in learning from imbalanced data. It introduces a new loss function used during the balancing training phase, which mitigates the influence of samples that contribute to an overfitted decision boundary.

- **Logit Adjustment (LA)** [23] proposes two methods for modifying the standard softmax cross-entropy training based on label frequencies. In this study, we select the post-hoc adjustment for logits, which entails applying post-event logarithmic probability adjustment to the trained model.
- **BLV** [36] introduces category-wise variation during the training phase for semantic segmentation. This perturbation is highly dependent on the category scale, resulting in smaller variations assigned to head classes and larger variations assigned to tail classes.

(2) two significant **comprehensive frameworks** for long-tailed learning:

- **MELT** [16] proposes a novel framework for sequential recommender systems that jointly addresses the long-tailed problem from the perspectives of both users and items. The framework consists of bilateral branches, each responsible for long-tailed users and items, respectively, and is effectively trained using a curriculum learning-based approach.
- **LoTNext** [7] integrates a long-tailed graph adjustment module that mitigates the effects of long-tailed nodes in user-POI interaction graphs, along with a long-tailed loss adjustment module that modifies loss calculations through strategies such as logit scoring and sample weight adjustments. Furthermore, auxiliary prediction tasks are incorporated to enhance its performance.

C.3 Evaluation Metrics

We evaluate model performance using the Mean Reciprocal Rank ($MRR@k$) and the Normalized Discounted Cumulative Gain ($NDCG@k$). $MRR@k$ is computed as follows:

$$MRR_u@k = \begin{cases} \frac{1}{r_u}, & \text{if } r_u \leq k, \\ 0, & \text{otherwise,} \end{cases} \quad (13)$$

where r_u represents the rank of the correct label for user u . $NDCG@k$ is computed as follows:

$$NDCG_u@k = \begin{cases} \frac{1}{\log_2(1+r_u)}, & \text{if } r_u \leq k, \\ 0, & \text{otherwise.} \end{cases} \quad (14)$$

C.4 Implementation Details

In this section, we provide additional details regarding the experimental settings. All experiments are conducted on a single NVIDIA RTX A6000 GPU, employing the Adam optimizer. A random seed of 42 is utilized across all experiments to ensure reproducibility. (1) **Four Backbone Architectures.** For Graph-Flashback, both the hidden states and the user (location) embeddings are configured with a dimensionality of 128. In STHGCN, the ID embedding dimension d_{id} for all check-in features is fixed at 128, a 2-layer hypergraph convolution model is employed, featuring a residual beta rate of 0.5 and 4 attention heads. In MCLP, the representation vectors are set to 128 dimensions, and the number of latent topics N^o in Latent Dirichlet Allocation (LDA) is 400, where the Transformer employs two stacked encoder layers with a 0.3 dropout rate and four attention heads in the multi-head attention module. In Diff-POI, the embedding size is set to 64 and the hyperparameters α , γ and λ are set to 0.5, 0.2 and 10^{-3} , respectively. The two interval thresholds, δ_s and δ_t , are both fixed at 256. Additionally, a step size of 0.01 is employed, which implies that the reversed Stochastic Differential Equation (SDE) for the sampling module is solved from time step 0 to 1 with $dt = 0.01$ at each step. (2) **Ours and Five Plugin Baselines.** The temperature for the Gumbel-Softmax in our proposed method is fixed at 1. Weight initialization for the four hierarchical levels is set to $\{1, 0.75, 0.5, 0.25\}$, corresponding to fine to coarse granularity. For the Focal Loss (Focal), the weights for head and tail classes are set to 1 and 2, respectively, with γ set to 2. In the case of Class-Balanced (CB) Loss, β is set to 0.9999 and the γ is set to 2. To mitigate numerical instability during the calculation of the Influence-balanced (IB) Loss, ϵ is set to 0.001. Given the slower convergence of the IB loss, we increase the training epochs on the backbone architectures. The parameter τ of Logit Adjustment (LA) is set to 1 to regulate the extent of adjustments made to the model logits. The Balancing Logit Variation (BLV) Loss employs a logarithmic ratio variation parameter σ of 4. (3) **Two Comprehensive Framework Baselines.** In LoTNext, location and user embeddings are set to 128 dimensions, while the time embedding dimension is 32. The Transformer architecture includes four multi-head attention mechanisms and one encoder block. For MELT, the hidden dimension is set to 128, the maximum sequence length is 200, λ_U and λ_I are both set to 0.1, with the model trained for 100 epochs using 2 transformer layers, which has a learning rate of 0.001 and betas of (0.9, 0.98).

D Gradient Analysis

In this section, we present a detailed gradient analysis focusing on the derivatives of our proposed Adaptive Hierarchical Loss (AHL) with respect to the logits in the location classification layer of any backbone architecture. For simplicity, we analyze the derivative of a prediction concerning the logits.

D.1 Initial Probability Derivative

We denote the logit for the label y_j^H as z_j . For any class from the leaf nodes, its initial probability is defined as follows:

$$p_0(y_i^H) = \frac{\exp\left(\frac{z_i+g_i}{\tau}\right)}{\sum_{k=1}^{C^H} \exp\left(\frac{z_k+g_k}{\tau}\right)}. \quad (15)$$

Since $\mathbf{z} = \sum_{k=1}^{C^H} \exp\left(\frac{z_k+g_k}{\tau}\right)$, we can differentiate $p_0(y_i^H)$ with respect to z_j using the quotient rule:

$$\begin{aligned} \frac{\partial p_0(y_i^H)}{\partial z_j} &= \frac{\partial}{\partial z_j} \left(\frac{\exp\left(\frac{z_i+g_i}{\tau}\right)}{\mathbf{z}} \right) \\ &= \frac{\mathbf{z} \cdot \frac{\partial}{\partial z_j} \exp\left(\frac{z_i+g_i}{\tau}\right) - \exp\left(\frac{z_i+g_i}{\tau}\right) \cdot \frac{\partial \mathbf{z}}{\partial z_j}}{\mathbf{z}^2} \\ &= \frac{\mathbf{z} \cdot \frac{1}{\tau} \exp\left(\frac{z_i+g_i}{\tau}\right) - \exp\left(\frac{z_i+g_i}{\tau}\right) \cdot \frac{1}{\tau} \sum_{k=1}^{C^H} \exp\left(\frac{z_k+g_k}{\tau}\right)}{\mathbf{z}^2} \\ &= p_0(y_i^H)(\delta_{ij} - p_0(y_i^H)), \end{aligned} \quad (16)$$

where δ_{ij} is the Kronecker delta function, which equals 1 when $i = j$ and 0 otherwise.

D.2 Hierarchical Conditional Probability Derivative

Let y_j^h be the label at the h -th hierarchical level. For simplicity, we introduce the variant S_i^h to represent the sum of probabilities of all leaf nodes of the non-leaf node y_i^h . The conditional probability for any class y_i^h at level h is given by:

$$p(y_i^h | y_i^{h-1}) = \frac{S_i^h}{S_i^{h-1}}, \quad S_i^h = \sum_{y_k^H \in \text{Leaves}(y_i^h)} p_0(y_k^H). \quad (17)$$

The derivative of this conditional probability with respect to z_j can be expressed as:

$$\frac{\partial p(y_i^h | y_i^{h-1})}{\partial z_j} = \frac{\partial S_i^h}{\partial z_j} \cdot \frac{1}{S_i^{h-1}} - \frac{S_i^h}{(S_i^{h-1})^2} \cdot \frac{\partial S_i^{h-1}}{\partial z_j}. \quad (18)$$

Here, we expand the derivative of S_i^h with respect to z_j :

$$\frac{\partial S_i^h}{\partial z_j} = \sum_{y_k^H \in \text{Leaves}(y_i^h)} \frac{\partial p_0(y_k^H)}{\partial z_j}. \quad (19)$$

We need to consider two situations. If $y_i^H \in \text{Leaves}(y_i^h)$, then:

$$\begin{aligned} \frac{\partial S_i^h}{\partial z_j} &= p_0(y_i^H)(1 - p_0(y_i^H)) - \sum_{y_k^H \in \text{Leaves}(y_i^h) \cap y_k^H \neq y_i^H} p_0(y_k^H)p_0(y_i^H) \\ &= p_0(y_i^H)(1 - S_i^h). \end{aligned} \quad (20)$$

Otherwise:

$$\frac{\partial S_i^h}{\partial z_j} = -S_i^h p_0(y_i^H). \quad (21)$$

D.3 Adaptive Hierarchical Loss Function Derivative

The conditional probability $p(y_i^h | y_i^{h-1})$ depends on z_i if and only if the node y_i^h is an ancestor of the leaf node y_i^H . Let the ancestral path of y_i^H be $\{y_i^1, y_i^2, \dots, y_i^H\}$. The loss function is defined as:

$$\ell_{\text{hier}} = - \sum_{h=1}^H w_i^h \log p(y_i^h | y_i^{h-1}). \quad (22)$$

The derivative of the loss function with respect to z_j is given by:

$$\begin{aligned} \frac{\partial \ell_{\text{hier}}}{\partial z_j} &= \sum_{h=1}^H w_i^h \cdot \frac{1}{p(y_i^h | y_i^{h-1})} \cdot \frac{\partial p(y_i^h | y_i^{h-1})}{\partial z_j} \\ &= - \sum_{h=1}^H w_i^h \left[\frac{1}{S_i^h} \cdot \frac{\partial S_i^h}{\partial z_j} - \frac{1}{S_{h-1}} \cdot \frac{\partial S_{h-1}}{\partial z_j} \right] \\ &= -w_i^1 \left[\frac{1}{S_i^1} \frac{\partial S_i^1}{\partial z_j} - 0 \right] - w_i^2 \left[\frac{1}{S_i^2} \frac{\partial S_i^2}{\partial z_j} - \frac{1}{S_i^1} \frac{\partial S_i^1}{\partial z_j} \right] \\ &\quad - w_i^3 \left[\frac{1}{S_i^3} \frac{\partial S_i^3}{\partial z_j} - \frac{1}{S_i^2} \frac{\partial S_i^2}{\partial z_j} \right] - w_i^4 \left[\frac{1}{S_i^4} \frac{\partial S_i^4}{\partial z_j} - \frac{1}{S_i^3} \frac{\partial S_i^3}{\partial z_j} \right] \\ &= -w_i^1 \frac{1}{S_i^1} \frac{\partial S_i^1}{\partial z_j} - \frac{w_i^2}{S_i^2} \frac{\partial S_i^2}{\partial z_j} + \frac{w_i^2}{S_i^1} \frac{\partial S_i^1}{\partial z_j} - \frac{w_i^3}{S_i^3} \frac{\partial S_i^3}{\partial z_j} + \frac{w_i^3}{S_i^2} \frac{\partial S_i^2}{\partial z_j} - \frac{w_i^4}{S_i^4} \frac{\partial S_i^4}{\partial z_j} + \frac{w_i^4}{S_i^3} \frac{\partial S_i^3}{\partial z_j} \quad (23) \\ &= \frac{\partial S_i^1}{\partial z_j} \left(\frac{w_i^2 - w_i^1}{S_i^1} \right) + \frac{\partial S_i^2}{\partial z_j} \left(\frac{w_i^3 - w_i^2}{S_i^2} \right) + \frac{\partial S_i^3}{\partial z_j} \left(\frac{w_i^4 - w_i^3}{S_i^3} \right) - \frac{w_i^4}{S_i^4} \frac{\partial S_i^4}{\partial z_j} \\ &= p_0(y_i^H)(1 - S_i^1) \cdot \frac{w_i^2 - w_i^1}{S_i^1} + p_0(y_i^H)(1 - S_i^2) \cdot \frac{w_i^3 - w_i^2}{S_i^2} \\ &\quad + p_0(y_i^H)(1 - S_i^3) \cdot \frac{w_i^4 - w_i^3}{S_i^3} - \frac{w_i^4}{S_i^4} p_0(y_i^H)(1 - S_i^4) \\ &= p_0(y_i^H) \left[\sum_{h=1}^{H-1} \frac{w_i^{h+1} - w_i^h}{S_i^h} + w_i^1 \right] - w_i^H \\ &= p_0(y_i^H) \cdot A - w_i^H, \end{aligned}$$

where $A = \sum_{h=1}^{H-1} \frac{w_i^{h+1} - w_i^h}{S_i^h} + w_i^1$. Through this gradient analysis, we gain insights into how adjustments in the logits influence the probabilities and loss function across the hierarchical structure, which is crucial for understanding and optimizing our model's training dynamics.

E More Experimental Results

In this section, we present more experimental results to further analyze the flexibility and effectiveness of our proposed ALOHA.

E.1 Overall Performance

The complete results of all methods across seven metrics over six datasets are presented in Table 5, 6, 7, 8, 9, and 10. In particular, we include the AVG metric to facilitate a clear comparison of their performance. Our method consistently demonstrates superior performance across all seven metrics, validating its effectiveness and generalizability across various backbone architectures. For the JKT dataset, ALOHA achieves an improvement of 9.40% on the MRR@1 metric using the Diff-POI backbone compared to the second-best baseline, Focal, indicating its robustness relative to other methods. For the KLP dataset, BLV exhibits the second-best performance on most backbone architectures (*i.e.*, Graph-Flashback, STHGCN, and MCLP), suggesting better adaptability in the mobility prediction task compared to other plugins designed for the computer vision field. For the MAO, MOW, and MEX datasets, most plugins experience a notable decline in performance compared

Table 5: MRR@ k and NDCG@ k performance of all methods on the JKT dataset. AVG is the average rank across seven metrics. **Bold** and underline mean the best and the second-best ranks.

Model	MRR@1	MRR@5	MRR@10	MRR@20	NDCG@5	NDCG@10	NDCG@20	AVG
Graph-Flashback	0.1916	0.2791	0.2909	0.2962	0.3164	0.3452	0.3646	<u>2.6</u>
+ Focal	0.1955	0.2800	0.2919	0.2975	0.3150	0.3435	0.3641	2.7
+ CB	0.1645	0.2387	0.2489	0.2536	0.2699	0.2947	0.3120	6.0
+ IB	0.1487	0.2205	0.2288	0.2324	0.2495	0.2695	0.2824	7.0
+ LA	0.1721	0.2474	0.2580	0.2628	0.2783	0.3042	0.3214	5.0
+ BLV	0.1874	0.2781	0.2897	0.2947	0.3151	0.3437	0.3619	3.7
+ Ours	0.2042	0.2893	0.3012	0.3066	0.3242	0.3530	0.3726	1.0
STHGCN	0.1976	0.2768	0.2878	0.2934	0.3101	0.3365	0.3566	3.3
+ Focal	0.1950	0.2782	0.2878	0.2937	0.3124	0.3358	0.3570	<u>2.7</u>
+ CB	0.1734	0.2422	0.2519	0.2566	0.2701	0.2938	0.3113	5.7
+ IB	0.1558	0.2239	0.2316	0.2362	0.2521	0.2707	0.2874	7.0
+ LA	0.1708	0.2424	0.2518	0.2569	0.2724	0.2953	0.3142	5.3
+ BLV	0.1966	0.2773	0.2883	0.2935	0.3109	0.3375	0.3562	2.9
+ Ours	0.2097	0.2899	0.3002	0.3058	0.3239	0.3487	0.3691	1.0
MCLP	0.1968	0.2796	0.2908	0.2958	0.3131	0.3400	0.3585	<u>2.0</u>
+ Focal	0.1961	0.2771	0.2881	0.2937	0.3102	0.3364	0.3569	3.0
+ CB	0.1792	0.2517	0.2621	0.2667	0.2822	0.3073	0.3237	6.9
+ IB	0.1839	0.2559	0.2649	0.2689	0.2859	0.3076	0.3219	6.0
+ LA	0.1834	0.2577	0.2679	0.2725	0.2892	0.3140	0.3305	5.1
+ BLV	0.1918	0.2763	0.2868	0.2927	0.3101	0.3357	0.3568	4.0
+ Ours	0.2045	0.2860	0.2966	0.3020	0.3194	0.3451	0.3647	1.0
Diff-POI	0.1234	0.1826	0.1912	0.1949	0.2070	0.2273	0.2408	4.1
+ Focal	0.1287	0.1865	0.1955	0.1994	0.2105	0.2321	0.2461	<u>2.1</u>
+ CB	0.1282	0.1826	0.1876	0.1898	0.2046	0.2167	0.2249	4.7
+ IB	0.0824	0.0981	0.1007	0.1021	0.1049	0.1112	0.1164	7.0
+ LA	0.1147	0.1677	0.1748	0.1780	0.1903	0.2072	0.2190	6.0
+ BLV	0.1289	0.1843	0.1928	0.1966	0.2087	0.2289	0.2427	2.9
+ Ours	0.1408	0.1950	0.2035	0.2067	0.2180	0.2385	0.2505	1.0
MELT	0.1388	0.2276	0.2399	0.2460	0.2632	0.2936	0.3158	<u>2.0</u>
LoTNext	0.1779	0.2568	0.2676	0.2724	0.2904	0.3164	0.3339	1.0

Table 6: MRR@ k and NDCG@ k performance of all methods on the KLP dataset. AVG is the average rank across seven metrics. **Bold** and underline mean the best and the second-best ranks.

Model	MRR@1	MRR@5	MRR@10	MRR@20	NDCG@5	NDCG@10	NDCG@20	AVG
Graph-Flashback	0.1729	0.2591	0.2703	0.2763	0.2950	0.3221	0.3439	4.0
+ Focal	0.1853	0.2630	0.2753	0.2817	0.2957	0.3252	0.3486	3.0
+ CB	0.1502	0.2147	0.2260	0.2309	0.2432	0.2700	0.2883	6.0
+ IB	0.1318	0.1936	0.2034	0.2070	0.2198	0.2435	0.2565	7.0
+ LA	0.1522	0.2219	0.2321	0.2372	0.2516	0.2764	0.2950	5.0
+ BLV	0.1881	0.2680	0.2796	0.2854	0.3027	0.3305	0.3514	<u>2.0</u>
+ Ours	0.1945	0.2744	0.2854	0.2914	0.3079	0.3345	0.3561	1.0
STHGCN	0.1961	0.2708	0.2826	0.2880	0.3025	0.3312	0.3509	2.9
+ Focal	0.1829	0.2602	0.2719	0.2772	0.2927	0.3207	0.3401	4.0
+ CB	0.1346	0.2006	0.2101	0.2146	0.2285	0.2515	0.2675	5.3
+ IB	0.0639	0.1056	0.1127	0.1170	0.1245	0.1414	0.1573	7.0
+ LA	0.1198	0.1942	0.2067	0.2125	0.2264	0.2563	0.2774	5.7
+ BLV	0.1937	0.2744	0.2858	0.2905	0.3092	0.3367	0.3536	<u>2.1</u>
+ Ours	0.2065	0.2836	0.2946	0.2996	0.3163	0.3431	0.3610	1.0
MCLP	0.1833	0.2594	0.2703	0.2755	0.2909	0.3174	0.3363	3.0
+ Focal	0.1713	0.2508	0.2616	0.2669	0.2830	0.3094	0.3285	4.0
+ CB	0.1554	0.2237	0.2336	0.2382	0.2523	0.2763	0.2930	5.9
+ IB	0.1534	0.2171	0.2247	0.2277	0.2439	0.2626	0.2733	7.0
+ LA	0.1554	0.2258	0.2362	0.2414	0.2547	0.2800	0.2989	5.0
+ BLV	0.1885	0.2627	0.2725	0.2780	0.2946	0.3186	0.3386	<u>2.0</u>
+ Ours	0.1937	0.2665	0.2774	0.2827	0.2968	0.3235	0.3429	1.0
Diff-POI	0.1250	0.1762	0.1843	0.1882	0.1973	0.2170	0.2314	2.9
+ Focal	0.1242	0.1794	0.1875	0.1921	0.2021	0.2214	0.2382	<u>2.1</u>
+ CB	0.1078	0.1605	0.1650	0.1674	0.1814	0.1922	0.2008	5.1
+ IB	0.1166	0.1378	0.1401	0.1419	0.1466	0.1522	0.1587	6.7
+ LA	0.0998	0.1511	0.1559	0.1595	0.1723	0.1841	0.1974	6.1
+ BLV	0.1194	0.1707	0.1785	0.1836	0.1920	0.2109	0.2293	4.0
+ Ours	0.1346	0.1901	0.1970	0.2008	0.2132	0.2297	0.2434	1.0
MELT	0.1139	0.1962	0.2072	0.2127	0.2314	0.2573	0.2775	<u>2.0</u>
LoTNext	0.1721	0.2423	0.2534	0.2593	0.2735	0.2999	0.3215	1.0

Table 7: MRR@ k and NDCG@ k performance of all methods on the MAO dataset. AVG is the average rank across seven metrics. **Bold** and underline mean the best and the second-best ranks.

Model	MRR@1	MRR@5	MRR@10	MRR@20	NDCG@5	NDCG@10	NDCG@20	AVG
Graph-Flashback	0.2093	0.3175	0.3315	0.3362	0.3631	0.3967	0.4135	2.9
+ Focal	0.1962	0.3107	0.3249	0.3295	0.3588	0.3923	0.4088	4.0
+ CB	0.1858	0.2824	0.2951	0.2988	0.3243	0.3548	0.3684	6.0
+ IB	0.1816	0.2793	0.2917	0.2961	0.3218	0.3514	0.3672	7.0
+ LA	0.1882	0.2879	0.2998	0.3044	0.3311	0.3598	0.3762	5.0
+ BLV	0.2093	0.3196	0.3338	0.3387	0.3657	0.3994	0.4170	<u>2.0</u>
+ Ours	0.2163	0.3316	0.3426	0.3469	0.3797	0.4060	0.4215	1.0
STHGCN	0.2281	0.3406	0.3522	0.3564	0.3869	0.4143	0.4291	<u>2.0</u>
+ Focal	0.2248	0.3356	0.3470	0.3508	0.3831	0.4103	0.4241	4.0
+ CB	0.2013	0.3031	0.3125	0.3159	0.3470	0.3693	0.3816	6.0
+ IB	0.1962	0.3012	0.3110	0.3148	0.3446	0.3680	0.3814	7.0
+ LA	0.2173	0.3225	0.3321	0.3360	0.3676	0.3904	0.4047	5.0
+ BLV	0.2262	0.3392	0.3504	0.3542	0.3862	0.4128	0.4264	3.0
+ Ours	0.2346	0.3448	0.3562	0.3600	0.3902	0.4175	0.4311	1.0
MCLP	0.2163	0.3285	0.3406	0.3455	0.3744	0.4036	0.4213	<u>2.0</u>
+ Focal	0.2088	0.3250	0.3358	0.3408	0.3726	0.3983	0.4164	3.3
+ CB	0.1957	0.2981	0.3097	0.3129	0.3419	0.3696	0.3810	6.1
+ IB	0.2004	0.2863	0.2942	0.2972	0.3214	0.3395	0.3503	6.9
+ LA	0.2023	0.3079	0.3198	0.3236	0.3520	0.3804	0.3941	5.0
+ BLV	0.2126	0.3228	0.3357	0.3406	0.3675	0.3984	0.4161	3.7
+ Ours	0.2210	0.3345	0.3459	0.3511	0.3802	0.4072	0.4260	1.0
Diff-POI	0.1455	0.2148	0.2230	0.2267	0.2439	0.2638	0.2769	<u>2.4</u>
+ Focal	0.1394	0.2105	0.2187	0.2224	0.2408	0.2609	0.2739	4.1
+ CB	0.1300	0.1967	0.2037	0.2061	0.2252	0.2416	0.2505	6.1
+ IB	0.1450	0.1790	0.1827	0.1852	0.1927	0.2015	0.2105	6.4
+ LA	0.1314	0.1982	0.2073	0.2102	0.2273	0.2490	0.2598	5.1
+ BLV	0.1427	0.2138	0.2226	0.2269	0.2429	0.2640	0.2795	2.7
+ Ours	0.1624	0.2287	0.2367	0.2406	0.2562	0.2752	0.2893	1.0
MELT	0.1940	0.3111	0.3221	0.3259	0.3616	0.3877	0.4012	1.1
LoTNext	0.1980	0.3076	0.3206	0.3249	0.3537	0.3850	0.4004	<u>1.9</u>

Table 8: MRR@ k and NDCG@ k performance of all methods on the MOW dataset. AVG is the average rank across seven metrics. **Bold** and underline mean the best and the second-best ranks.

Model	MRR@1	MRR@5	MRR@10	MRR@20	NDCG@5	NDCG@10	NDCG@20	AVG
Graph-Flashback	0.1752	0.2644	0.2737	0.2778	0.3017	0.3240	0.3388	<u>2.0</u>
+ Focal	0.1679	0.2618	0.2711	0.2747	0.3001	0.3225	0.3356	3.9
+ CB	0.1576	0.2414	0.2504	0.2537	0.2764	0.2983	0.3101	6.0
+ IB	0.1428	0.2290	0.2394	0.2416	0.2634	0.2882	0.2963	7.0
+ LA	0.1654	0.2510	0.2608	0.2637	0.2862	0.3096	0.3198	5.0
+ BLV	0.1719	0.2630	0.2729	0.2768	0.2998	0.3236	0.3380	3.1
+ Ours	0.1846	0.2738	0.2824	0.2861	0.3103	0.3309	0.3445	1.0
STHGCN	0.1815	0.2629	0.2722	0.2753	0.2963	0.3186	0.3301	3.0
+ Focal	0.1772	0.2623	0.2707	0.2741	0.2968	0.3171	0.3297	3.9
+ CB	0.1643	0.2405	0.2484	0.2510	0.2708	0.2897	0.2989	6.0
+ IB	0.1553	0.2268	0.2339	0.2365	0.2551	0.2723	0.2816	7.0
+ LA	0.1665	0.2426	0.2512	0.2545	0.2741	0.2947	0.3069	5.0
+ BLV	0.1784	0.2639	0.2724	0.2756	0.2989	0.3196	0.3312	<u>2.1</u>
+ Ours	0.1846	0.2705	0.2786	0.2818	0.3051	0.3248	0.3362	1.0
MCLP	0.1770	0.2616	0.2714	0.2748	0.2964	0.3197	0.3319	3.6
+ Focal	0.1761	0.2648	0.2735	0.2766	0.3009	0.3216	0.3327	<u>2.4</u>
+ CB	0.1641	0.2482	0.2567	0.2598	0.2830	0.3033	0.3143	6.1
+ IB	0.1757	0.2426	0.2480	0.2498	0.2690	0.2817	0.2884	6.9
+ LA	0.1788	0.2634	0.2713	0.2745	0.2978	0.3166	0.3281	3.9
+ BLV	0.1770	0.2618	0.2712	0.2746	0.2966	0.3192	0.3318	4.0
+ Ours	0.1871	0.2723	0.2813	0.2845	0.3071	0.3286	0.3402	1.0
Diff-POI	0.1208	0.1781	0.1841	0.1862	0.2020	0.2165	0.2244	<u>2.0</u>
+ Focal	0.1159	0.1723	0.1781	0.1804	0.1957	0.2096	0.2182	3.1
+ CB	0.1128	0.1668	0.1715	0.1735	0.1880	0.1992	0.2066	5.1
+ IB	0.0871	0.1029	0.1058	0.1074	0.1100	0.1170	0.1227	7.0
+ LA	0.1045	0.1632	0.1681	0.1703	0.1870	0.1987	0.2068	5.9
+ BLV	0.1166	0.1699	0.1767	0.1792	0.1916	0.2078	0.2169	3.9
+ Ours	0.1302	0.1840	0.1905	0.1928	0.2058	0.2215	0.2299	1.0
MELT	0.1348	0.2189	0.2283	0.2329	0.2539	0.2765	0.2930	<u>2.0</u>
LoTNext	0.1837	0.2626	0.2713	0.2745	0.2955	0.3159	0.3275	1.0

Table 9: MRR@ k and NDCG@ k performance of all methods on the SPB dataset. AVG is the average rank across seven metrics. **Bold** and underline mean the best and the second-best ranks.

Model	MRR@1	MRR@5	MRR@10	MRR@20	NDCG@5	NDCG@10	NDCG@20	AVG
Graph-Flashback	0.2019	0.2959	0.3061	0.3113	0.3338	0.3583	0.3771	4.0
+ Focal	0.2128	0.3011	0.3105	0.3159	0.3367	0.3592	0.3791	<u>2.3</u>
+ CB	0.2001	0.2889	0.2964	0.3007	0.3250	0.3430	0.3583	5.9
+ IB	0.1658	0.2599	0.2709	0.2743	0.2975	0.3238	0.3361	7.0
+ LA	0.1977	0.2898	0.2989	0.3028	0.3274	0.3489	0.3630	5.1
+ BLV	0.2098	0.3003	0.3099	0.3145	0.3383	0.3611	0.3775	2.7
+ Ours	0.2260	0.3121	0.3223	0.3270	0.3476	0.3725	0.3896	1.0
STHGCN	0.1844	0.2754	0.2846	0.2892	0.3119	0.3338	0.3503	5.9
+ Focal	0.1935	0.2823	0.2915	0.2959	0.3184	0.3408	0.3565	3.0
+ CB	0.1977	0.2832	0.2911	0.2949	0.3182	0.3376	0.3509	3.4
+ IB	0.1875	0.2769	0.2861	0.2892	0.3131	0.3351	0.3466	5.3
+ LA	0.1887	0.2832	0.2929	0.2962	0.3195	0.3424	0.3545	<u>2.4</u>
+ BLV	0.1869	0.2729	0.2823	0.2871	0.3076	0.3307	0.3479	6.7
+ Ours	0.2007	0.2857	0.2953	0.2998	0.3204	0.3436	0.3600	1.0
MCLP	0.2031	0.2925	0.3011	0.3060	0.3298	0.3503	0.3679	4.1
+ Focal	0.2025	0.2938	0.3025	0.3061	0.3312	0.3521	0.3651	3.4
+ CB	0.1971	0.2863	0.2949	0.2976	0.3217	0.3422	0.3518	6.1
+ IB	0.1977	0.2777	0.2851	0.2867	0.3084	0.3258	0.3318	6.9
+ LA	0.2001	0.2936	0.3030	0.3059	0.3291	0.3516	0.3621	4.4
+ BLV	0.2086	0.2969	0.3057	0.3098	0.3339	0.3554	0.3701	<u>2.0</u>
+ Ours	0.2158	0.3042	0.3128	0.3167	0.3408	0.3617	0.3760	1.0
Diff-POI	0.1332	0.2070	0.2133	0.2171	0.2357	0.2509	0.2647	3.1
+ Focal	0.1368	0.2089	0.2167	0.2187	0.2390	0.2576	0.2650	<u>2.1</u>
+ CB	0.1272	0.1958	0.2024	0.2050	0.2235	0.2390	0.2481	6.0
+ IB	0.1200	0.1502	0.1539	0.1558	0.1624	0.1714	0.1784	7.0
+ LA	0.1290	0.1968	0.2043	0.2073	0.2244	0.2427	0.2528	5.0
+ BLV	0.1374	0.2026	0.2113	0.2146	0.2284	0.2488	0.2608	3.7
+ Ours	0.1543	0.2242	0.2305	0.2328	0.2518	0.2667	0.2751	1.0
MELT	0.1630	0.2562	0.2645	0.2691	0.2933	0.3136	0.3303	<u>2.0</u>
LoTNext	0.1911	0.2784	0.2890	0.2937	0.3150	0.3406	0.3576	1.0

Table 10: MRR@ k and NDCG@ k performance of all methods on the MEX dataset. AVG is the average rank across seven metrics. **Bold** and underline mean the best and the second-best ranks.

Model	MRR@1	MRR@5	MRR@10	MRR@20	NDCG@5	NDCG@10	NDCG@20	AVG
Graph-Flashback	0.1989	0.2905	0.3000	0.3033	0.3279	0.3508	0.3628	<u>2.0</u>
+ Focal	0.1836	0.2804	0.2899	0.2937	0.3193	0.3422	0.3557	4.0
+ CB	0.1565	0.2452	0.2555	0.2591	0.2822	0.3068	0.3196	6.0
+ IB	0.1517	0.2375	0.2468	0.2501	0.2739	0.2964	0.3081	7.0
+ LA	0.1703	0.2582	0.2680	0.2714	0.2955	0.3186	0.3307	5.0
+ BLV	0.1915	0.2846	0.2942	0.2975	0.3229	0.3461	0.3580	3.0
+ Ours	0.2053	0.2979	0.3072	0.3106	0.3353	0.3577	0.3699	1.0
STHGCN	0.1971	0.2845	0.2928	0.2960	0.319	0.3391	0.3505	<u>2.1</u>
+ Focal	0.1812	0.2661	0.2744	0.2777	0.3009	0.3207	0.3328	4.0
+ CB	0.1469	0.2237	0.2311	0.2338	0.2548	0.2725	0.2819	5.9
+ IB	0.0851	0.1305	0.1380	0.1411	0.1509	0.1689	0.1801	7.0
+ LA	0.1424	0.2295	0.2391	0.2424	0.2668	0.2898	0.3016	5.1
+ BLV	0.2008	0.2819	0.2902	0.2938	0.3143	0.3342	0.3471	2.9
+ Ours	0.2050	0.2913	0.2988	0.3023	0.3264	0.3447	0.3576	1.0
MCLP	0.2019	0.2871	0.2951	0.2981	0.3221	0.3413	0.3523	<u>2.0</u>
+ Focal	0.1958	0.2824	0.2912	0.2941	0.3178	0.3388	0.3492	3.9
+ CB	0.1782	0.2646	0.2727	0.2758	0.3011	0.3204	0.3314	6.0
+ IB	0.1743	0.2605	0.2696	0.2726	0.2972	0.3190	0.3295	7.0
+ LA	0.1854	0.2722	0.2815	0.2842	0.3083	0.3305	0.3405	5.0
+ BLV	0.1966	0.2834	0.2913	0.2947	0.3193	0.3381	0.3505	3.1
+ Ours	0.2072	0.2903	0.2990	0.3020	0.3246	0.3450	0.3558	1.0
Diff-POI	0.1180	0.1739	0.1794	0.1826	0.1963	0.2094	0.2207	3.7
+ Focal	0.1263	0.1771	0.1831	0.1853	0.1976	0.2121	0.2201	<u>2.1</u>
+ CB	0.0997	0.1518	0.1582	0.1602	0.1733	0.1884	0.1957	5.4
+ IB	0.0496	0.0662	0.0693	0.0712	0.0733	0.0809	0.0879	7.0
+ LA	0.0966	0.1515	0.1577	0.1602	0.1740	0.1887	0.1978	5.4
+ BLV	0.1255	0.1761	0.1819	0.1843	0.1972	0.2112	0.2198	3.1
+ Ours	0.1329	0.1835	0.1886	0.1908	0.2046	0.2168	0.2248	1.0
MELT	0.1573	0.2407	0.2489	0.2526	0.2747	0.2947	0.3081	<u>2.0</u>
LoTNext	0.1846	0.2723	0.2808	0.2844	0.3082	0.3284	0.3416	1.0

with the basic version, indicating their inadequacy for mobility prediction involving more complex spatiotemporal modeling. SPB is the sparsest dataset, where Focal, LA, and BLV represent the second-best baseline across different backbone architectures; however, our method consistently outperforms all others, highlighting the robustness of ALOHA. Additionally, the Diffusion-based backbone (*i.e.*, Diff-POI) performs poorly relative to other backbone architectures on nearly all datasets, suggesting its limitation in executing long-tail mobility prediction with greater data sparsity. For two comprehensive framework used in long-tailed recommendation system and mobility prediction task, due to the inherent difference of scales and strategies, MELT is worse than that of the basic versions of most backbones involving spatiotemporal modeling. In the two comprehensive frameworks used for long-tailed recommendation systems and mobility prediction tasks, MELT performs worse than the basic versions of most backbone architectures involving spatiotemporal modeling due to inherent differences in scales and strategies.

E.2 Further Analysis

E.2.1 Weights Analysis

Figure 14, 15, 16, 17, 18 illustrate the optimized weights obtained by the “STHGCN + Ours” model across five additional datasets, revealing distinct patterns in weight distribution and correlation coefficients between head and tail locations. In these datasets, the weight distribution for tail locations is more concentrated, and the weight values are larger, indicating a greater degree of optimization for these locations. In contrast, head locations often exhibit lower and more dispersed weights, suggesting that the degree of optimization for head locations is dynamically adjusted according to the varying characteristics of human mobility. For most datasets, the correlation coefficient between adjacent hierarchical levels is relatively high, underscoring the necessity of constructing a progressive hierarchical tree structure. Head locations typically have higher correlation coefficients than tail locations, indicating that frequently visited locations maintain closer weights across different hierarchical levels. These visualization results demonstrate the model’s ability to dynamically adjust for unbalanced locations in the long-tailed mobility prediction task. These findings highlight the

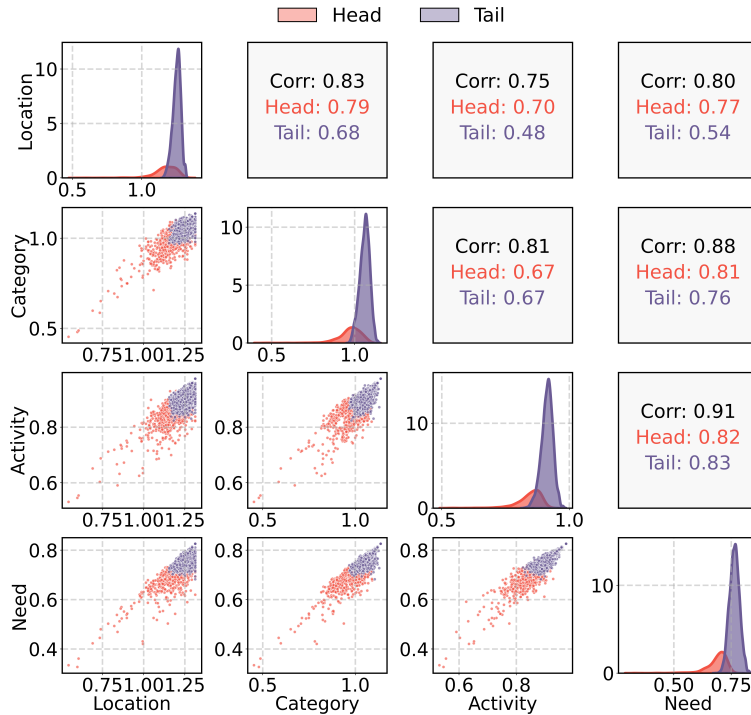


Figure 14: Optimized hierarchical weights of ALOHA on the KLP dataset.

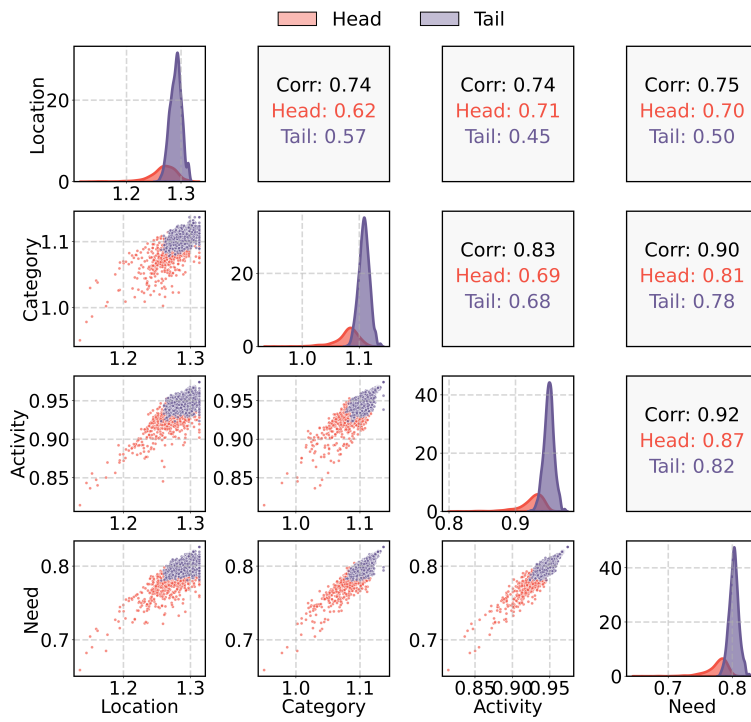


Figure 15: Optimized hierarchical weights of ALOHA on the MAO dataset.

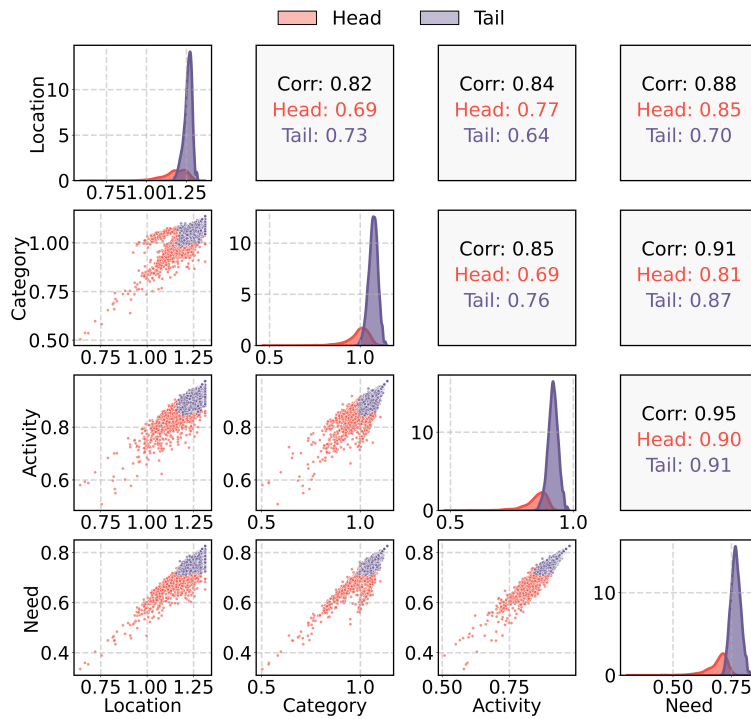


Figure 16: Optimized hierarchical weights of ALOHA on the MOW dataset.

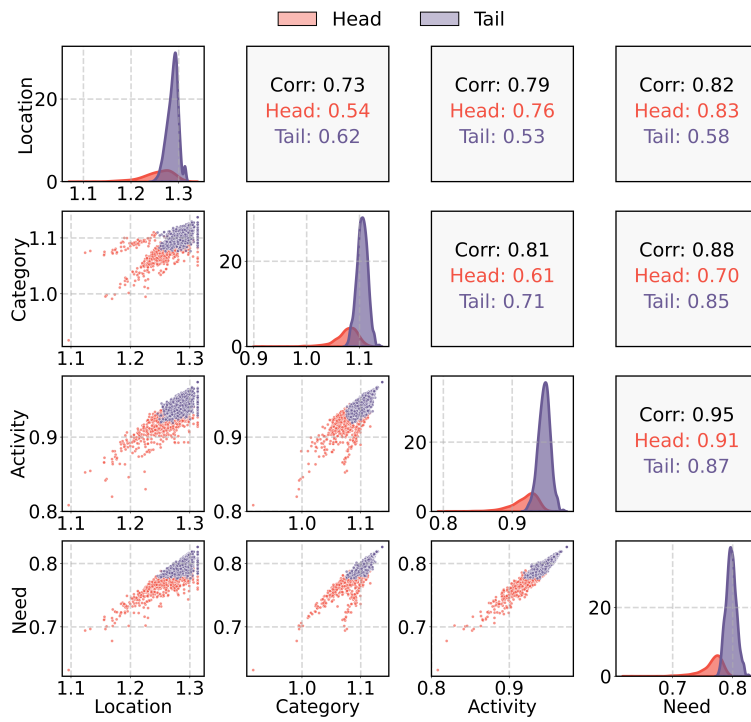


Figure 17: Optimized hierarchical weights of ALOHA on the SPB dataset.

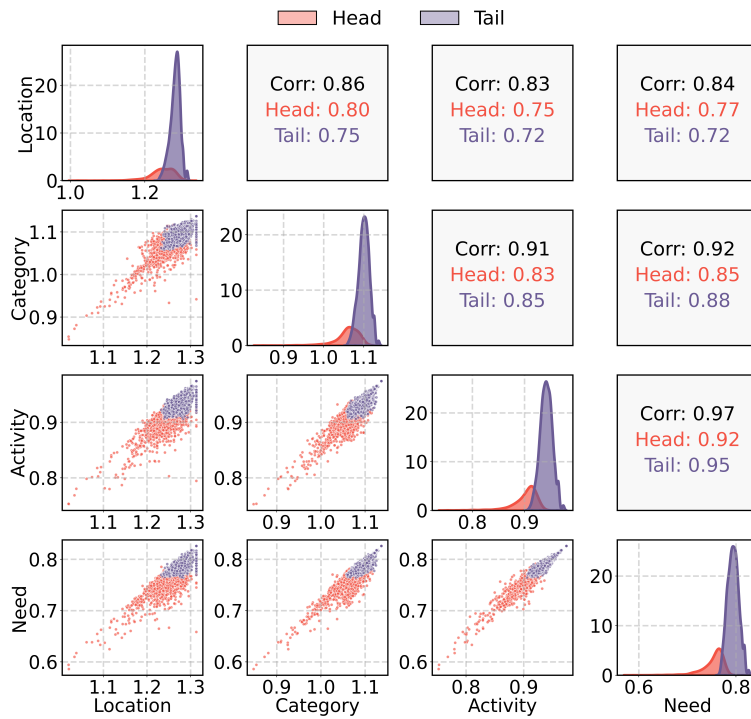


Figure 18: Optimized hierarchical weights of ALOHA on the MEX dataset.

effectiveness of adaptive hierarchical learning in our proposed ALOHA model, promote adaptive adjustments for dynamic spatiotemporal semantic modeling, and enhance overall performance.

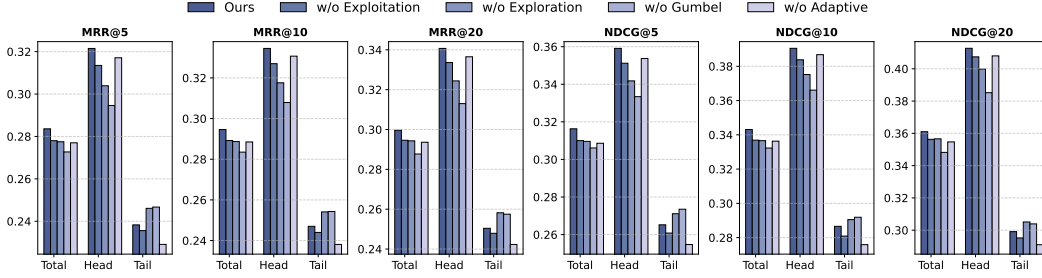


Figure 19: Ablation study of our proposed ALOHA using STHGCN backbone on KLP dataset.

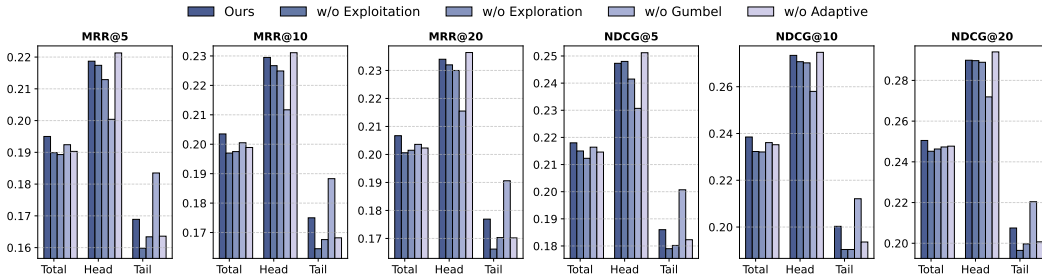


Figure 20: Ablation study of our proposed ALOHA using Diff-POI backbone on the JKT dataset.

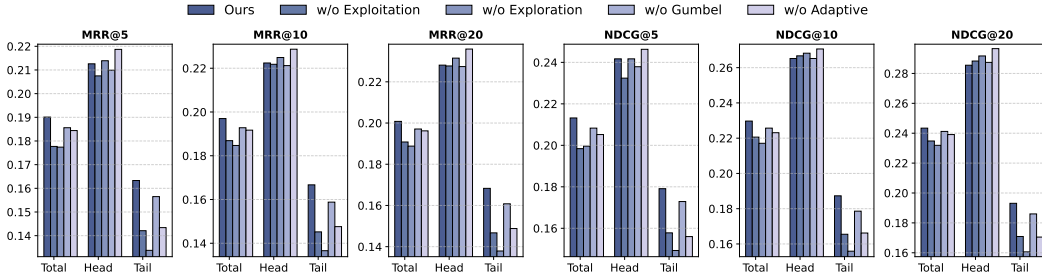


Figure 21: Ablation study of our proposed ALOHA using Diff-POI backbone on KLP dataset.

E.2.2 Ablation Study

We present the results of the ablation studies for the best backbone architecture (*i.e.*, STHGCN) and the worst backbone architecture (*i.e.*, Diff-POI) on the JKT and KLP datasets. As illustrated in Figure 6, 19, 20, 21, our proposed ALOHA achieves the best performance across total locations for both backbone architectures and datasets, with all variants outperforming the second-best results presented in Table 2, confirming the consistent effectiveness of ALOHA. For the results on the STHGCN backbone architecture over the KLP dataset and the Diff-POI backbone architecture over the JKT dataset, the variant “w/o Gumbel” performs worse than all other variants on head locations but outperforms the others on tail locations, indicating the effectiveness of the overall hierarchical learning framework for the long-tailed mobility prediction task. The performance of “w/o Adaptive” contrasts with that of “w/o Gumbel”, suggesting the comprehensiveness and complementarity of the exploration mechanism in our proposed ALOHA. The “w/o Exploitation” and “w/o Exploration” variants on the Diff-POI backbone across both datasets lead to notable degradation in performance on tail locations, demonstrating the necessity of mobility knowledge exploitation and exploration in our proposed ALOHA.

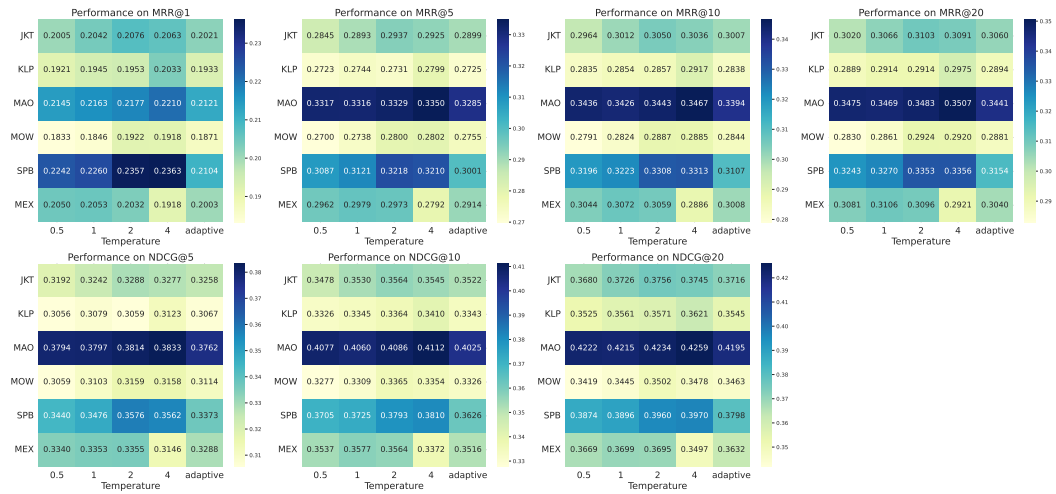


Figure 22: The impact of parameter τ in our proposed ALOHA using RNN-based backbone (Graph-Flashback) across six datasets.

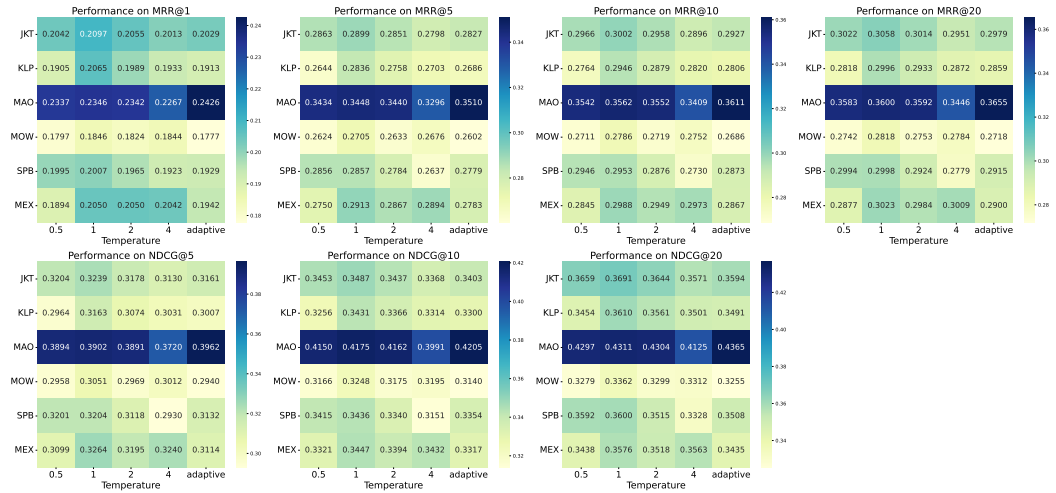


Figure 23: The impact of parameter τ in our proposed ALOHA using GNN-based backbone (STHGCN) across six datasets.

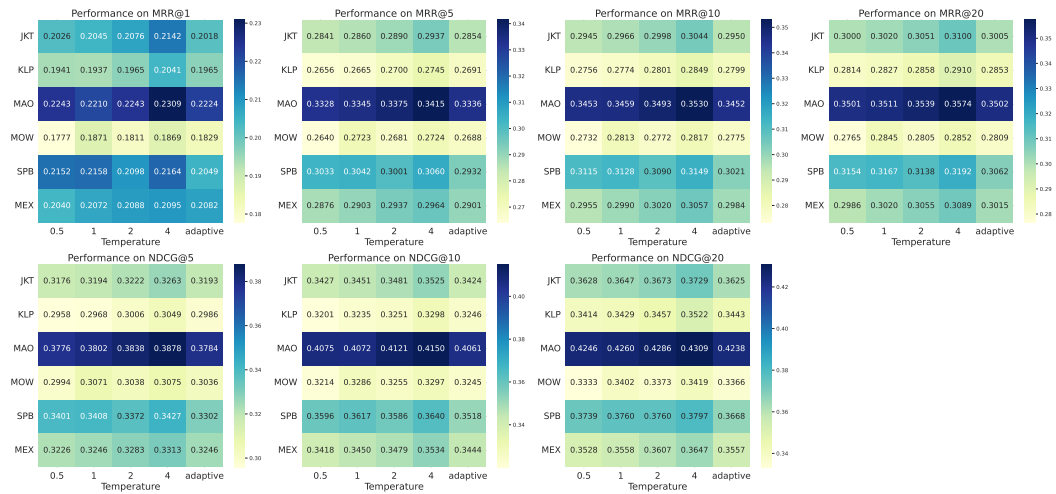


Figure 24: The impact of parameter τ in our proposed ALOHA using Transformer-based backbone (MCLP) across six datasets.

E.2.3 Hyperparameter Analysis

Temperature τ is a significant parameter in the Gumbel disturbance of our proposed ALOHA, as it controls the smoothness of the predicted logits involving Gumbel noise, thereby rebalancing the predictions for head and tail locations. To study the impact of τ on ALOHA, we conduct experiments with five settings: four fixed values (0.5, 1, 2, 4) and one adaptive strategy ranging from 2 to 0.5 across three relatively advanced backbone architectures (*i.e.*, Graph-Flashback, STHGCN, and MCLP) on six datasets. Figure 22, 23, 24 present their performance across seven metrics including $MRR@k$ and $NDCG@k$. We observe that the performance of our proposed ALOHA is robust to various values of the temperature parameter τ . For the Graph-Flashback backbone architecture, we surprisingly find that it achieves better performance than reported in Table 2 by adjusting the temperature τ from 1 to 2 on the JKT and MOW datasets, and from 1 to 4 on the KLP, MAO and SPB datasets, demonstrating the potential of our proposed ALOHA for long-tailed mobility prediction. In comparison to the other two backbone architectures, STHGCN is less sensitive to the temperature parameter τ , achieving the best results at $\tau = 1$ on most datasets. For the Transformer-based backbone architecture, it outperforms with $\tau = 1$ on the MOW dataset and with $\tau = 4$ on the other five datasets.

E.3 Computational Cost

As shown in Table 11, we analyze the computational efficiency of ALOHA and plugin baselines across four backbone architectures. Most plugins, including our model, add minimal computational overhead compared to base versions. BLV is the slowest plugin due to its normal distribution generation step, while Base, Focal, CB share overlapping computations and thus similar speeds. LA shows marginally higher costs on MCLP and Graph-Flashback due to matrix addition operations. Among the four backbone architectures, MCLP demonstrates the fastest training time due to its structural simplicity. In contrast, Graph-Flashback’s $O(N^2)$ spatiotemporal flashback mechanism slightly reduces its speed. STHGCN incurs additional overhead from multi-hop neighbor sampling, whereas Diff-POI’s continuous-time stochastic differential equations (SDE) framework requires multi-step sampling, making it the slowest backbone. Plugin baselines (excluding BLV) exhibit minor runtime variations across architectures, influenced by the dimension of sequence length in MCLP and Graph-Flashback compared to STHGCN and Diff-POI.

Table 11: The average computation time of each trajectory of all plugin baselines across four backbone architectures on the JKT dataset, measured in units of 10^{-3} second.

Model	Graph-Flashback	STHGCN	MCLP	Diff-POI
Base	0.628	8.492	0.437	12.753
+ Focal	0.709	8.782	0.447	12.950
+ CB	0.644	8.613	0.466	13.267
+ IB	0.709	8.534	0.521	12.662
+ LA	0.727	8.480	0.544	12.708
+ BLV	4.978	8.969	4.918	13.879
+ Ours	0.735	8.824	0.514	12.889

F Broader Impacts

Our proposed ALOHA enhances mobility prediction by addressing long-tailed distributions, thereby offering societal benefits such as equitable urban planning and sustainable infrastructure development through balanced predictions for both high-demand and low-demand locations. Its generalizability across cities has the potential to democratize access to mobility tools in data-limited regions, promoting fairness in location-based services. We acknowledge the privacy risks associated with the deployment of ALOHA. If implemented in institutions lacking stringent data protection measures, reliance on extensive user mobility data may result in privacy breaches, potentially leading to adverse social impacts such as unauthorized surveillance or misuse of personal data. By analyzing both the potential benefits and risks, we provide a broader perspective on its impacts, aligning with the transparency and accountability standards of artificial intelligence research.